Retinoic acid receptor beta protects striatopallidal medium spiny neurons from mitochondrial dysfunction and neurodegeneration

Marion Ciancia [a,b,c,d,1], Monika Rataj-Baniowska [a,b,c,d,1], Nicolas Zinter [a,b,c,d],
Vito Antonio Baldassarro [a,b,c,d,i], Valérie Fraulob [a,b,c,d], Anne-Laure Charles [e], Rosana Alvarez [f],
Shin-ichi Muramatsu [g,h], Angel R. de Lera [f], Bernard Geny [e], Pascal Dollé [a,b,c,d],
Anna Niewiadomska-Cimicka [a,b,c,d], Wojciech Kręzel [a,b,c,d,*]

[a] Institut de Génétique et de Biologie Moléculaire et Cellulaire (IGBMC), 67404 Illkirch, France
[b] Inserm, U 1258, 67404 Illkirch, France
[c] CNRS UMR 7104, 67404 Illkirch, France
[d] Université de Strasbourg, 67404 Illkirch, France
[e] Institut de Physiologie, Faculté de Médecine, "Mitochondrie, Stress Oxydant et Protection Musculaire", 4 Rue Kirschleger, 67085 Strasbourg, France
[f] Departamento de Química Orgánica, Facultade de Química, CINBIO and IBIV, Universidade de Vigo, Campus As Lagoas-Marcosende, 36310 Vigo, Spain
[g] Division of Neurological Gene Therapy, Center for Open Innovation, Jichi Medical University, Tochigi 3290498, Japan
[h] Center for Gene and Cell Therapy, The Institute of Medical Science, The University of Tokyo, Tokyo 1088639, Japan
[i] Department of Veterinary Medical Science (DIMEVET), University of Bologna, Ozzano Emilia (Bologna), Italy

ARTICLE INFO

ABSTRACT

Retinoic acid is a powerful regulator of brain development, however its postnatal functions only start to be elucidated. We show that retinoic acid receptor beta (RARβ), is involved in neuroprotection of striatopallidal medium spiny neurons (spMSNs), the cell type affected in different neuropsychiatric disorders and particularly prone to degenerate in Huntington disease (HD). Accordingly, the number of spMSNs was reduced in the striatum of adult *Rarβ⁻/⁻* mice, which may result from mitochondrial dysfunction and neurodegeneration. Mitochondria morphology was abnormal in mutant mice whereas in cultured striatal *Rarβ⁻/⁻* neurons mitochondria displayed exacerbated depolarization, and fragmentation followed by cell death in response to glutamate or thapsigargin-induced calcium increase. *In vivo*, *Rarβ⁻/⁻* spMSNs were also more vulnerable to the mitochondrial toxin 3-nitro-propionic acid (3NP), known to induce HD symptoms in human and rodents. In contrary, an RARβ agonist, AC261066, decreased glutamate-induced toxicity in primary striatal neurons *in vitro*, and diminished mito-chondrial dysfunction, spMSN cell death and motor deficits induced in wild type mice by 3NP. We demonstrate that the striatopallidal pathway is compromised in *Rarβ⁻/⁻* mice and associated with HD-like motor abnormalities. Importantly, similar motor abnormalities and selective reduction of spMSNs were induced by striatal or spMSN-specific inactivation of RARβ, further supporting a neuroprotective role of RARβ in postnatal striatum.

1. Introduction

All-*trans*-retinoic acid (ATRA) is a powerful morphogen and key determinant of vertebrate development. During brain ontogenesis, its widespread effects reflect specific, complementary or redundant expression and activities of retinoic acid receptors (RAR α, β, γ) acting as ATRA-dependent transcription factors. RARβ is one of the most abundantly expressed receptors and such expression is restricted almost exclusively to the developing and adult striatum. Analyses of *Rarβ⁻/⁻* mice carrying null mutation of RARβ revealed its specific contribution to

formation of striosomes, the key structural component of the striatum (Liao et al., 2008) as well as striatonigral medium spiny neurons (snMSNs) expressing dopamine D1 receptor (*Drd1*) and tachynin 1 (*Tac1*) (Rataj-Baniowska et al., 2015). These neurons together with striatopallidal medium spiny neurons (spMSNs) expressing dopamine D2 receptor (*Drd2*) and proenkephaline (*Penk*) constitute the two main output projection neurons in the striatum. In contrast to the developmental functions of RARβ, its role in the adult striatum remains unknown despite its expression in mouse and human striatum. Unravelling its functions might be relevant for understanding of a number of neuropsychiatric disorders associated with striatal dysfunctions (Crittenden and Graybiel, 2011). In particular, RARβ expression was strongly decreased in the striatum of Huntington disease (HD) patients (Hodges et al., 2006) and animal models (Lee et al., 2020; Luthi-Carter et al., 2000; Niewiadomska-Cimicka et al., 2011), raising the possibility that such decrease may contribute to the physiopathology of HD. Importantly, decreased RARβ expression was recently reported the top predicted regulator of the downregulated genes in both types of MSNs in patients and the *mHtt* Q175KI and R6/2 mouse models of HD (Lee et al., 2020).

Huntington disease (HD) is an autosomal dominant neurologic disease caused by expansion of CAG trinucleotide repeats in the first exon of the huntingtin (Htt) gene. Despite ubiquitous expression of mutant Htt (mHtt), the brain−and in particular the striatum−is the most severely affected tissue, exhibiting prominent structural atrophy and cell loss. The physiopathological mechanisms leading to HD are not clear, although unbalanced signaling of snMSNs and spMSNs has been suggested to underlie core motor symptoms of the disease and their evolution. In particular, in early phases of the disease, preferential loss of spMSNs expressing *Penk* and *Drd2* has been reported in post-mortem samples (Albin et al., 1992; Deng et al., 2004; Reiner et al., 1988; Richfield et al., 1995) and by longitudinal PET imaging studies of HD patients (Niccolini et al., 2018), and could lead to compromised activity of the striatonigral pathway and uncontrolled movements (chorea).

The specific mechanisms underlying the dysfunction and high vulnerability of spMSNs to cell death are not known, but a number of hypotheses have been proposed based on studies of animal models of HD. Several mouse models (the transgenic R6/1, R6/2, YAC128 or knock-in Q175KI lines) reproduced HD-like motor abnormalities including early hyperactivity followed by hypoactivity and motor coordination deficits (Bolivar et al., 2004; Luesse et al., 2001; Slow et al., 2003; Smith et al., 2014). However, loss of MSNs was reported only in YAC128, Q175KI and R6/2 models of HD (Slow et al., 2003; Smith et al., 2014), although snMSN *vs* spMSN cell loss was not investigated. The cause of cell death in those models is not known, though it may reflect an increased vulnerability of MSNs to degenerate in response *e.g.* to glutamatergic excitotoxicity, as suggested by *in vitro* and *in vivo* studies (Cepeda et al., 2001; Estrada Sanchez et al., 2008; Fernandes et al., 2007; Hodgson et al., 1999; Mattis et al., 2015; Zeron et al., 2002). Mitochondrial dysfunction and associated abnormal calcium signalling were postulated as causal factors of such enhanced vulnerability but also overall metabolic defects observed in HD (Dubinsky, 2017; Mochel et al., 2012; Mochel and Haller, 2011). Accordingly, enlarged mitochondria were observed in fibroblasts or myoblasts (Panov et al., 2002; Squitieri et al., 2010) and either bigger or fragmented mitochondria in neurons (Fernandes et al., 2007; Hodgson et al., 1999; Jin et al., 2013; Kim et al., 2010; Martinez-Vicente et al., 2010). Thus, considering the high energetic demand of MSNs, mitochondrial defects were proposed to underlie preferential MSN degeneration in HD (Ferrante et al., 1991; Mitchell and Griffiths, 2003), although such hypothesis did not explain the differential susceptibility of spMSNs *vs* snMSNs. Analyses of several HD animal models revealed decreased mitochondrial respiration (electron transport chain activity), Ca^{2+} buffering capacity and ATP production (reviewed in (Oliveira, 2010)). Importantly, abrogation of complex II activity by 3-nitropropionic acid (3-NP) was shown sufficient to induce specific striatal degeneration with cell death of MSNs and

HD-like behavioral abnormalities in wild type rodents (Blum et al., 2003; Page et al., 2000; Sun et al., 2002) and in human (Ludolph et al., 1991). Decreased succinate dehydrogenase (SDH) activity (the molecular target of 3-NP-mediated inhibition) was reported in HD patients (Browne et al., 1997; Gu et al., 1996; Tabrizi et al., 1999) and directly linked with mHtt-dependent mitochondrial dysfunction and cell death (Benchoua et al., 2006). In particular, increased Ca^{2+} levels following activation of NMDA receptors, or inhibition of Ca^{2+} uptake by the endoplasmic reticulum, were shown in mice or cultured cells expressing mHtt to result in exacerbated rise of reactive oxygen species (ROS), mitochondrial fragmentation and apoptotic cell death ((Quintanilla et al., 2013; Quintanilla et al., 2017) and references therein).

Since cell loss was not observed in all animal models despite presence of HD-like phenotypes, it was suggested that dysfunction of MSNs prior to or without MSN cell death may also contribute to unbalanced signaling of direct *vs* indirect striatal output pathways. For example, compromised Drd2 signaling was detected in the R6/2 mouse model in the absence of cell death (Spektor et al., 2002), whereas increased input resistance, excitability and altered perception of glutamatergic signalling were differentially affected in spMSNs and snMSNs in YAC128 or Q175 KI mice prior to cell death (Andre et al., 2011; Goodliffe et al., 2018). In support of early and functionally relevant dysfunction of MSNs in HD are transcriptional changes which magnitude and extent correlate with the length of CAG repeats and behavioral abnormalities in the allelic series of *Htt* KI mice (Langfelder et al., 2016). Such graded correlations concerned in particular genes involved in cell identity and associated mostly with spMSNs, but also transcripts relevant for cAMP signalling, mitochondrial functions, cell death, synaptic connectivity and transcription factors affected in HD. This wide range of functional abnormalities in HD may reflect direct interactions of wild type (WT) and/or mutant Htt with DNA, mitochondria, chromatin modifiers or transcription factors resulting in control of distinct cell processes. In this context, we have previously shown that sequestration of RARβ by mutant Htt in R6/2 mice was associated with compromised transcription of a large array of RARβ transcriptional targets, recapitulating a subset of changes observed in HD patients and mouse models (Niewiadomska-Cimicka et al., 2017). The most severely affected transcripts were associated with cell identity, calcium homeostasis, cAMP signalling and mitochondrial functions.

We report here morphological and functional deficits in mitochondria of *Rarβ*−/− striatal cells which may directly underlie loss of a subpopulation of spMSNs and in consequence hypoactivity of the indirect pathway and HD-like motor abnormalities which we observed in *Rarβ*−/− mice. In support of this hypothesis, we found that subthreshold levels of mitochondrial toxin 3-NP exacerbated spMSN cell death in *Rarβ*−/− mice, whereas AC261066, an agonist of RARβ, prevented loss of *Drd2* + spMSNs and attenuated motor deficits in 3-NP-treated WT mice. The RARβ agonist also prevented mitochondrial depolarization, fragmentation and cell death in WT cultured striatal neurons exposed to glutamatergic excitotoxicity. Globally, these data point to a postnatal role of RARβ in neuroprotection of spMSNs, which is further supported by progressive motor deficits and loss of *Drd2* + spMSNs following conditional RARβ inactivation in the adult striatum or specifically in Drd2 + spMSNs. RARβ-dependent neuroprotection might be of relevance for understanding of the physiopathology of HD and pave the way for new treatment strategies.

2. Materials and methods

2.1. Animals

Mice carrying a null mutation for *Rarβ* (*Rarβ*−/−) were generated from heterozygous crosses as previously described (Ghyselinck et al., 1997). All mice were on homogeneous mixed genetic background of about 50% C57BL6J and 50% 129svEmx for more than 10 generations. For conditional inactivation of *Rarβ* we used mice carrying floxed exon 9 and 10

coding for the DNA binding domain which were generated on 83% C57BL6J and 17% 129svpas background as previously described (Chapellier et al., 2002). $Rar\beta^{Drd2-/-}$ mice were generated by crossing floxed $Rar\beta$ mice with transgenic mice expressing Cre under control of Drd2 promoter (Gong et al., 2007). For all experiments mice were housed (3–4/cage) with water and food available *ad libitum* and 12 h/12 h light/dark cycle with the beginning of the light phase at 7 am. Male mice aged between 8 and 16 weeks were used for all functional, histological and molecular tests as indicated in the text, with exception of conditional RARβ knockout mice which were tested until 32 weeks of age. The experiments were approved by local ethics committee (project 2013–032 and 2018012610304876) and accredited by the French Ministry for Superior Education and Research in accordance with the Directive of the European Parliament: 2010/63/EU or were carried out in accordance with the European Community Council Directives of 24 November 1986 (86/609/EEC) and in compliance with the guidelines of CNRS and the French Agricultural and Forestry Ministry (decree 87848).

2.2. Behavior

Unless otherwise specified, behaviorally naive mice were tested in a battery of behavioral tests in order of presentation below and with 1–2 days of intervals between the tests according to standard operating procedures used at Mouse Clinical Institute.

2.2.1. Open-field test
Mice were tested in automated open field arenas (infrared sensors, Tru-Scan, Coulbourn). Briefly, mice were individually placed in the periphery of the open field and allowed to explore the apparatus freely for 30 min. The distance travelled, the number of rears and time spent in the central and peripheral regions were recorded over the test session. The test was performed in a room homogeneously illuminated at 70 Lux.

2.2.2. Spontaneous locomotion in actimetric cages
Spontaneous locomotor activity was measured in actimetric cages (Immetronic, Pessac, France). The duration of the experiment was 32 h (11 am until 7 pm the next day). Specifically, each mouse was placed in an individual cage equipped with infra-red photo beam cells on the side walls of the cage in order to measure the animal's horizontal movements. During the experiment mice had free access to food and water.

2.2.3. Locomotor coordination on the Rotarod
Accelerated (4–40 rpm in 5 min) rotarod (Bioseb, France) was used for all experiments. Each test consisted of three trials separated by 15–20 min recovery intervals. The latency time to fall from the rotarod was recorder. Unless mice fell from the rotating rod, to avoid habituation to passive turning on the rotarod, the cut off time was settled after 3rd passive rotation. Before the first trial mice were allowed to stay on the rotarod for about 30 s of habituation period before starting the acceleration phase.

2.2.4. Haloperidol-induced catalepsy
The bar test was used to examine haloperidol-induced catalepsy. During the test, both forelimbs of a mouse were placed on a horizontal bar 4 cm above the ground. Each animal underwent one session of the test (baseline/spontaneous catalepsy) prior to haloperidol treatment and subsequently at 30 and 60 min after haloperidol (IP) treatment. The time of immobility before stepping down the bar was considered as catalepsy score.

2.3. Pharmacology

Amphetamine, haloperidol, SKF81297 and 3-NP were purchased from Tocris Bio-Techne (France) and were dissolved in saline. All substances were administered by intraperitoneal injections. Amphetamine (3 mg/kg) and SKF81297 (1 mg/kg) were injected after 1 h habituation period in the actimetric cages (see spontaneous locomotion in actimetric cages) and activity was measured for additional 120 min for amphetamine and 60 min for SKF81297 treatment. During testing, food and water were not accessible. All mice treated with haloperidol (1 mg/kg) or SKF81297 were sacrificed at 90 min after treatment for analyses of cFos expression. 3-NP treatment was performed over two consecutive days and consisted of 4 injections delivered at 12 h intervals (7 am, 7 pm), attaining a total dose of 120, 200 or 280 mg/kg. AC261066 was synthetized according to previously reported procedures (Lund et al., 2009, 2005) and was dissolved in ethanol for *in vitro* experiments. For *in vivo* experiments, AC261066 was dissolved in sunflower oil and was injected at a dose of 2 mg/kg (2 ml/kg) 1 h before the injections of 3-NP or saline solution in case of control group.

2.4. Viral infections and analyses of conditional RARβ knockout mice

For viral infections we adapted previously reported protocol (Krzyzosiak et al., 2010). To this end, AAV9 vectors were engineered harboring a CAG promoter, the cDNA of interest, woodchuck hepatitis virus posttranscriptional regulatory element (WRPE; nucleotides 1093–1684, GenBank accession number J04514) and simian virus 40 polyadenylation signal sequence. This expression cassette was inserted between the inverted terminal repeats (ITR) of the AAV9 genome. For excision of floxed allele the expression cassette consisted of EGFPCre fusion protein to generate AAV9EGFPCre virus, whereas virus expressing EGFP only (AAV9EGFP) was generated to control of effects of viral infection. Recombinant AAV vectors were produced by transient transfection of human embryonic kidney (HEK293) cells and purified by isolation from two sequential continuous CsCl gradients, as previously described (Li et al., 2006). The titers of viral vectors were determined by quantitative PCR of DNase-I-treated vector stocks, and were estimated at 8.2×10^{12} viral genomes per milliliter (vg/ml) for AAV9EGFPCre and 4×10^{12} vg/ml for AAV9EGFP.

For experiments assessing conditional inactivation of RARβ we used in total 23 male mice carrying floxed alleles of $Rar\beta$. All mice were tested in the rotarod and actimetric cages one week prior to viral infections and were distributed semi-randomly into two groups to be injected with respective viral vectors at the age of 11 weeks. Following induction of deep anesthesia with intraperitoneal injection of ketamine (100 mg/kg)/xylazine (10 mg/kg), mice were placed in the stereotaxic frame (Precision Cinematographique, Paris, France) and injected bilaterally with 2 μl of viral suspension into the striatum (bregma = + 1.1; lateral = ± 1.5; ventral = +2.65 position in the Mouse Brain Atlas, (Paxinos and Franklin, 2001)). Following longitudinal behavioral testing in the rotarod and actimetric cages at 5, 10 and 20 weeks after viral injection all mice were sacrificed one week after the last test and their brains were frozen in cryomatrix for further analyses. The efficiency of viral infection was controlled by immunofluorescent analyses of bilateral expression of EGFP (to control of viral infection) and RARβ expression in control $Rar\beta^{AAV9EGFP}$ mice and its absence $Rar\beta^{AAV9EGFPCre}$ conditional knockout mice to control for efficiency of RARβ inactivation. Mice with inefficient bilateral or only unilateral infection were removed from further analyses. Finally, n = 8 out of 11 $Rar\beta^{AAV9EGFP}$ mice and n = 9 out of 12 $Rar\beta^{AAV9EGFPCre}$ mice were retained for behavioral analyses, out of which 6 mice of each group were used for analyses of cell types.

2.5. Mitochondrial respiration

Tissue was placed in an oxygraphic chamber at 37 °C, under stirring with 2 ml MiRO5 + creatine solution (EGTA 0.5 mM, MgCl$_2$ 3 mM, K lactobionate 60 mM, taurine 20 mM, KH$_2$PO$_4$ 10 mM, HEPES 20 mM, sucrose 110 mM), creatine 20 mM, BSA 1 g/l). Mitochondrial respiration was performed using a high-resolution oxygraph (Oxygraph-2k; Oroboros Instruments, Innsbruck, Austria). DatLab software 4.3 was used to measure the oxygen flux (Oroboros Instruments, Innsbruck).

After a basal signal, saponin was injected (50 μg/ml) to permeabilize

tissue. Then mitochondrial substrates or inhibitors were successively injected in the chamber in order to asses different complexes of the mitochondrial respiratory chain, namely glutamate (10 mM), malate (5 mM) and pyruvate (10 mM), and then ADP (5 mM), followed by succinate (10 mM) were injected to determine the maximal oxygen consumption. Then, rotenone (0.5 μM), an inhibitor of complex I, was injected. Finally, to measure complex IV activity, antimycin (2.5 μM) was injected (a complex III inhibitor) and complex IV was activated with injection of ascorbate (0.5 mM) and N′-tetramethyl-p-phenylenediamine dihydrochloride (TMPD, 0.5 mM). Data are expressed in pmol O_2/sec/ mg wet weight.

2.6. SDH enzymatic activity staining

For the analysis of SDH enzymatic activity, brains were dissected from WT and $Rar\beta^{-/-}$ mice, embedded in Shandon Cryomatrix (Thermo Scientific), frozen, and stored at $-80\,^\circ$C until sectioned. Cryosections (14 μm) were incubated in the staining solution (KH_2PO_4 20 mM, Na_2HPO_4 76 mM, sodium succinate 100 mM, NBT 0,1%) for 20 min at room temperature (RT). For mice treated with 3-NP, sections were incubated for 30 min to increase the signal in control mice. Brain sections were then fixed in 10% formalin for 10 min, rinsed 2 times in 15% ethanol, mounted in AquaMount and scanned for quantification with a Nanozoomer Scanner (Hamamatsu) in quantitative, TIFF mode. The intensity of the signal in the dorsolateral CPu was normalized by the intensity in the adjacent cortex.

2.7. In situ hybridization and cell counts

Cryosections were thawed and dried for 30 min at RT, post-fixed with 4% paraformaldehyde (PFA) dissolved in phosphate-buffered saline (PBS), acetylated with 0.1 M triethanolamine (TEA), rinsed with standard saline citrate (SSC), dehydrated by an increasing ethanol gradient, air-dried and hybridized at 65 °C overnight with digoxigenin-labelled RNA probes: *Rarβ* (full-length cDNA), *GAD67* (Erlander et al., 1991), *Drd1* (402 bp fragment of 3' region of *Drd1* cDNA), *Drd2* (1681 bp fragment of 5' region of *Drd2* cDNA), *pENK* (800 bp fragment of *pENK* cDNA covering *Hinc*II-*Xba*I region), *Tac1* (460 bp fragment covering the entire cDNA). After hybridization the sections were rinsed, blocked and incubated for 1 h at RT with an anti-digoxigenin, alkaline phosphatase-conjugated antibody (Roche). The sections were subsequently rinsed and incubated in the dark with a NBT/BCIP solution (Nitroblue tetrazolium chloride/ 5-bromo-4chloro-3-indyl-phosphate; Roche) until the staining appeared (overnight or up to 48 h). If the staining reaction was longer than overnight the NBT/BCIP solution was changed after 24 h.

Double labelling fluorescent *in situ* hybridization was performed as previously described (Etter and Krezel, 2014). The sections went through the same pre-hybridization steps as described above. For the hybridization reaction, two specific RNA probes (one digoxigenin- and the other fluorescein-labelled) were used to label corresponding mRNAs in the same tissue sample. The fluorescein-labelled RNA probe was detected using an anti-fluorescein antibody (Roche) coupled to horse-radish peroxidase and a cascade of amplification steps, including Tyramide Signal Amplification (TSA) with biotin followed by binding of Neutravidin-Oregon Green conjugates (Molecular Probes). After inactivation of remaining horseradish peroxidase activity, the digoxigenin-labelled probe was revealed using an anti-dig antibody coupled with horseradish peroxidase (Roche), which activity was detected with a TSA-CY3 kit (Perkin Elmer). The sections were rinsed and mounted with Aqua-Poly/Mount for subsequent imaging.

Imaging was performed using Nanozoomer digital scanner (Hamamatsu Photonics, France) or Leica M420 or DMLB/DM4000B microscopes equipped with Photometrics digital cameras and the CoolSnap imaging software (Roger Scientific). The cells were counted as previously described(Rataj-Baniowska et al., 2015). Briefly, the ROIs were

determined in dorsal striatum and nucleus accumbens shell as shown in Fig. 4A on at least three sections at corresponding brain levels between bregma 1.34 and 0.92. Cell counts were performed semi automatically using two approaches by two independent experimenters: (1) ImageJ software (Rasband, http://rsb.info.nih.gov/ij/) using 8-bit image mode and Point Selection with Light Background in "Find Maxima" process (Prominence - noise tolerance - set at 10) and (2) a software developed in the laboratory (M. Baniowski) and used previously(Rataj-Baniowska et al., 2015). Counting was manually curated to account for adjacent cells recognized as one object. Both methods gave similar results and mean of these two independent counts was used for analyses to calculate the number of cells per square millimeter.

2.8. Transmission electron microscopy

Mice were deeply anesthetised with a mix of ketamine and xylazine and perfused intracardiac with 10 ml of ice-cold PBS, followed by 20 ml of 4% PFA in PBS. Dorsolateral part of caudate putamen was dissected from 200 μm vibratome sections and was placed in 2.5% glutaraldehyde and 2.5% PFA in cacodylate buffer (0.1 M, pH 7.4) at 4 °C overnight. For morphological analysis by immersion in 1% osmium tetroxide in 0.1 mM cacodylate buffer for 1 h at 4 °C and dehydrated through graded ethanol (50%, 70%, 90% and 100%) and propylene oxide for 30 min each. The samples were embedded in Epon 812. Ultrathin sections were cut at 70 nm, contrast-strained with uranyl acetate and lead citrate and examined using a CM12 100Kv electron microscope. Images were captured digitally using a Orius1000 CCD camera (Gatan).

2.9. Cell cultures

Striatal primary neuronal cultures from lateral ganglionic eminence of E13.5 WT and $Rar\beta^{-/-}$ embryos were prepared according a previously described protocol (Rataj-Baniowska et al., 2015). Briefly, brains were removed, and striatum was isolated and incubated in non-enzymatic dissociation buffer (Sigma-Aldrich) for 15 min at 37 °C, followed by mechanical trituration by pipetting. Cells were counted, plated at a 250, 000 cell/well density, onto Cultrex 2D (0.25 mg/ml, Trevingen) coated coverslips in a 24 well plate (Falcon) and were maintained in a humidified incubator at 37 °C with 5% CO_2. Cells were analyzed after 7 days *in vitro* (DIV) for the vulnerability and rescue studies as described below.

2.10. Neuronal vulnerability

To study the vulnerability of striatal neurons, cells at 7 DIV were treated with 1 μM thapsigargin (Sigma-Aldrich) for 30, 60 or 90 min. A group not treated with thapsigargin (see time 0 min in Fig. 2B) was used as control group.

After thapsigargin treatment a LDH cytotoxicity assay (Pierce™, Thermofisher) was performed on the medium according to the manufacturer's instructions, and living cells were treated with 100 nM of MitoTracker Orange CMXRos® (ThermoFisher Scientific) for 15 min at 37 °C to report on mitochondrial membrane potential and networking. After a PBS washing step, cells were fixed in 4% PFA for 10 min at RT.

Cell images were acquired using SP8-UV confocal microscope (Leica, Germany). For MitoTracker intensity analysis, images were taken with a 40x objective, while for mitochondrial morphology analysis images were taken with a 63x objective with 4x zoom.

MitoTracker staining was quantified by Image-J software on the Maximum intenstity projection of the confocal z-stacks. A region of interest (ROI) of a fixed diameter was used to quantify the intensity of signal. At least 3 cells per images and 5 images per group were analyzed.

Mitochondria networking was analyzed by using IMARS software (Bitplane, Zurich, Switzerland). Three-dimensional images were elaborated in order to analyze the mean volume of the mitochondria network in the neurites. The software allows the building of an isosurface on a

specific section of the 3D image, identifying the mitochondria net. The mean volume of the individual mitochondria was used to quantify the mitochondria network. At least 3 images per coverslip were analyzed.

Moreover, in order to study neuronal sensitivity to glutamate toxicity and ROS production, striatal cultures at 7 DIV were treated for 10 min with 42 μM glutamate in Krebs buffer at 37 °C and 5% CO_2. Control cultures received Krebs buffer during this period. After glutamate treatment, Krebs buffer was replaced with the former culture medium and cells were incubated at 37 °C and 5% CO_2 for 24 h. At this point, cells were treated with CellROX Deep Red (ThermoFisher Scientific; 5 μM) for 30 min and during the last 15 min MitoTracker was added, as previously described. After incubation, cells were washed with PBS, fixed with 4% PFA for 10 min at RT, and stained for the MAP-2 marker as described below. For prevention of glutamate excitotoxicity with a RARβ agonist, 1 μM AC261066 or vehicle (ethanol) for control condition was applied 18 h prior to glutamate treatment.

For analyses, images of three random fields were acquired for each sample. 3D images were analyzed by IMARIS software (Bitplane, Concord, MA). An isosurface of MAP-2 staining was generated in order to recognize mature neurons in each culture. The MitoTracker and CellROX intensities were measured inside the generated isosurface in order to quantify mitochondrial depolarization and ROS. Mitochondrial network morphology was analyzed as described above.

2.11. Immunocytochemistry

Primary striatal cell cultures cultured on Coultrex-coated glass coverslips were fixed with 4% PFA for 10 min at RT, washed in PBS and incubated for 1 h with 1% BSA. Cells were rinsed with PBS and stained using as primary antibody chicken anti-MAP-2 (Abcam, France; 1:5000), mouse anti-NeuN (Millipore, France; 1:1000), rabbit anti-DARP32 (Synaptic Systems, Germany; 1:1000). Following washes with PBS, cultures were incubated with a secondary, anti-chicken, Alexa647- or Alexa488-conjugated antibody (Invitrogen, France; 1:500). Brain cryosections (14 μm) from virus-injected mice were thawed, dried and fixed with 4% PFA for 10 min at RT. Following washes and blocking steps, RARβ was detected using a polyclonal rabbit anti-RARβ antibody (1:500) and an anti-rabbit, Alexa555-conjugated secondary antibody as previously described (Niewiadomska-Cimicka et al., 2017). Nuclei were stained with DAPI in all experiments.

2.12. Western blotting

Striatum samples were homogenized manually in RIPA lysis buffer (Tris HCl 50 mM, NaCl 30 mM, EDTA 2 mM, Triton 0.01X) supplemented with a protease inhibitor cocktail (#11873580001, Roche Diagnostic). Samples were then sonicated (2 ×3 s) and left 30 min on ice. Following centrifugation, protein concentration was quantified using Bradford assay (#5000006, Biorad) and 20 μg of protein extracts were separated by SDS–PAGE, and electro-transferred (400 mA during 1 h) onto nitrocellulose membrane (#A29612452, Amersham 0.2 μm). Immunodetection was carried out using following antibodies: rabbit anti-RARβ, 1:1000 (Rochette-Egly et al., 1992); mouse anti-GAPDH, 1:5000 (CAB932Hu22, USCN) and horseradish peroxidase (HRP)-conjugated secondary antibodies (Goat anti-mouse, 1:5000, G-21040, Invitrogen; Goat anti-rabbit, 1:5000, #111 035 44, Jackson Immunoresearch). Enzymatic detection was carried out using Super Signal West Femto Maximum Sensitivity Substrate (#34095, Thermoscientific). GAPDH was used as a loading control when quantifying RARβ.

2.13. Statistical analyses

The comparisons of cell counts or specific treatments in mitochondrial respiration were carried out using student t-test. Mitochondrial size was analysed using Mann-Whitney test as data did not follow normal distribution as determined by Shapiro-Wilk test. The effects of specific treatments on WT *vs Rarβ* $^{-/-}$ or viral injections, or two different pharmacological treatments were analysed using two-way ANOVA with treatment and genotype, or AAV vector, or treatment type as independent variables. If measures were repeated for the same subjects (open field test, spontaneous locomotion in actimetric cages or longitudinal analyses of conditional inactivation *Rarβ*) ANOVA on repeated measures was used. All post-hoc analyses were performed using Bonferroni's multiple comparisons test.

3. Results

3.1. Mitochondria display morphological and functional deficits in Rarβ$^{-/-}$ striatum

Our previous ChIPseq data strongly suggested that RARβ might regulate genes involved in mitochondrial functions (Niewiadomska-Cimicka et al., 2017). To address this possibility in *Rarβ*$^{-/-}$ null mutants, we first investigated mitochondrial morphology using transmission electron microscopy, focusing on the dorsolateral striatum (Fig. 1A and B). Although some abnormal mitochondria exhibiting transparent or missing cristae were found in WT samples, the percentage of such abnormal mitochondria was significantly higher in *Rarβ*$^{-/-}$ mice attaining a mean of $39.90 \pm 1.91\%$ per cell, as compared to $13.09 \pm 1.10\%$ in WT (see also Fig. 1B). This increased number of defective mitochondria was not compensated by an overall increase of the mitochondrial number, which in fact showed rather significant decrease (0.447 ± 0.015 mitochondria per μm^2 of cytoplasm for *Rarβ*$^{-/-}$ and 0.504 ± 0.051 for WT; $p < 0.0001$, unpaired t-test). Importantly, the mean size of mutant mitochondria was increased by about 40% (0.165 ± 0.004 μm^2 in *Rarβ*$^{-/-}$ and 0.117 ± 0.003 μm^2 in WT; $p < 0.0001$, unpaired t-test; Fig. 1C), which was also supported by a tendency for increased surface of cytoplasm covered by mitochondria in mutant striatum ($7.228 \pm 0.22\%$ of the cytoplasm in *Rarβ*$^{-/-}$ and $5.775 \pm 0.52\%$ in WT; $p = 0.063$, unpaired t-test). Considering the important role of decreased mitochondrial complex II / SDH activity in HD physiopathology (Benchoua et al., 2006), we evaluated SDH enzymatic activity in the dorsolateral region of the striatum in WT and *Rarβ*$^{-/-}$ mice (see rectangles in Fig. 1D). Such activity expressed as ratio of signal intensity in the striatum with respect to the adjacent cortex was significantly lower in *Rarβ*$^{-/-}$ brains (Fig. 1E). Compromised functions of complex II were further supported by reduced mitochondrial respiration observed after addition of succinate, the SDH substrate, to *Rarβ*$^{-/-}$ samples in respirometry measures using high-resolution Oxygraph-2k (Fig. 1F).

3.2. Increased sensitivity to calcium-induced mitochondrial fragmentation and cell death in primary cultures of Rarβ$^{-/-}$ striatal neurons

Reduced SDH activity and mitochondrial respiration indicate mitochondrial dysfunction in *Rarβ*$^{-/-}$ striatum, which may lead to adaptive changes like increased mitochondrial size to ensure cell homeostasis and survival in resting conditions. We hypothesized that such survival might be compromised in challenge conditions. To address this possibility, we established primary MSN cultures from lateral ganglionic eminence at embryonic day E13.5 (Fig. S1) as previously described (Rataj-Baniowska et al., 2015) and challenged cultured WT and *Rarβ*$^{-/-}$ striatal cells with pathological calcium concentrations induced by thapsigargin treatment. This compound acts as an inhibitor of calcium uptake by the endoplasmic reticulum, and has been shown to induce excessive mitochondrial injury and cell death *via* mitochondrial permeability transition pore (mPTP) opening in MSNs expressing mutant huntingtin ((Quintanilla et al., 2013) and refs therein). By measuring signal intensity of MitoTracker (Fig. 2A, B), we found that in non-stimulated conditions membrane potential was higher in *Rarβ*$^{-/-}$ cells, possibly reflecting adaptive changes, but that addition of 1 μM thapsigargin dramatically decreased mitochondrial membrane potential in *Rarβ*$^{-/-}$ but not in WT MSNs ($F_{(3, 32)} = 11.15$, $p < 0.0001$ for interaction of treatment and
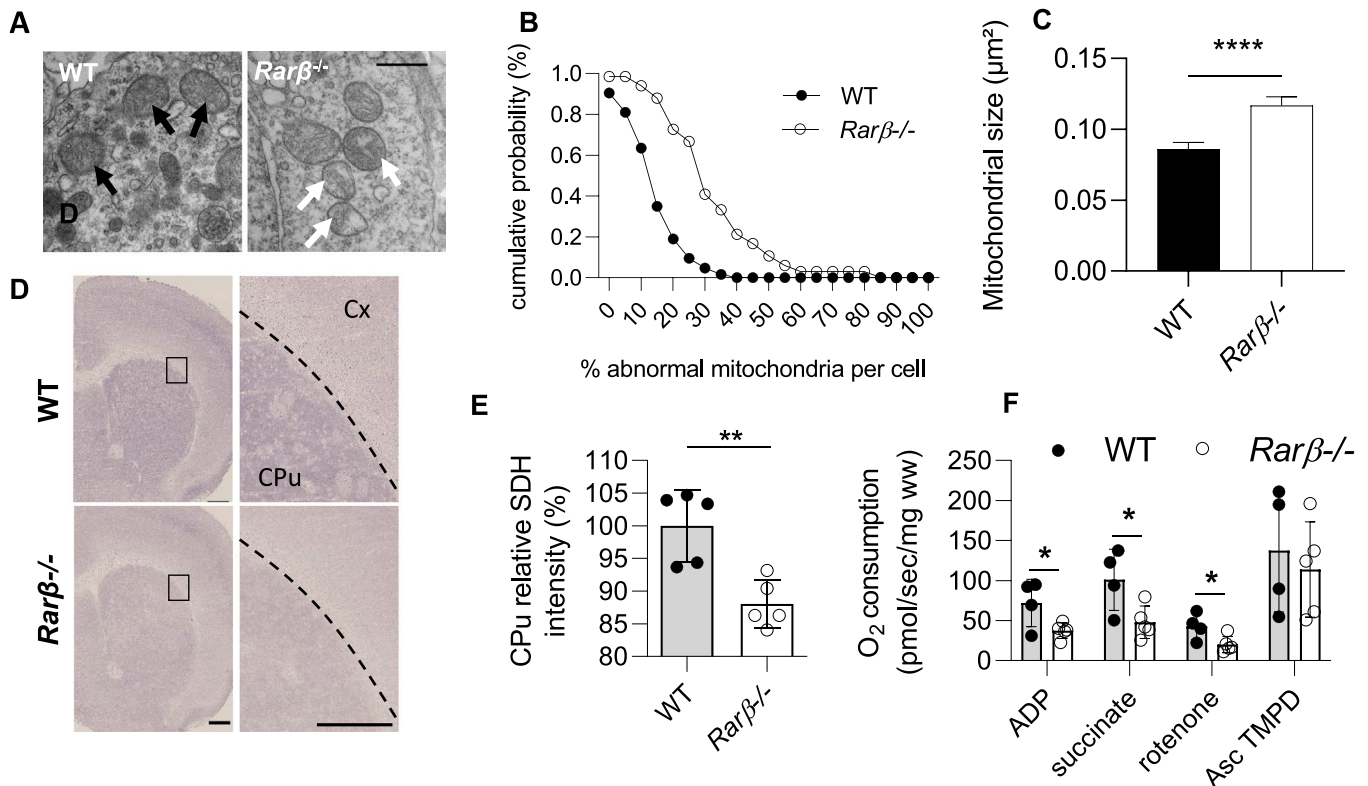
Fig. 1. Abnormal mitochondrial morphology and function in $Rar\beta^{-/-}$ striatum. (A) An example of transmission electron microscopy of mitochondria in WT (black arrows) and $Rar\beta^{-/-}$ neurons. White arrows indicate abnormal mitochondria with disrupted cristae. (B) Cumulative probability curve of abnormal mitochondria (disrupted cristae) quantified among n = 1701 WT and n = 1645 $Rar\beta^{-/-}$ mitochondria. (C) Mean mitochondrial surface. (D) An example of SDH enzymatic activity detection on brain sections of WT and $Rar\beta^{-/-}$ mice. (E) SDH intensity in the caudate putamen (Cpu) was quantified by normalization with respect to the intensity in the adjacent cortical region (Cx) and expressed as percent of cortical signal. (F) Respirometry performed on WT and $Rar\beta^{-/-}$ caudate putamen after addition of adenosine diphosphate (ADP), succinate, rotenone, and ascorbate + TMPD (Asc TMPD). * , p < 0.05; * *, p < 0.01; * ** *, p < 0.0001. Scale bars: (A) 2 μm and (D) 500 μm. Error bars represent standard error of means (SEM).

genotype). Importantly, decrease of the potential was observed in $Rar\beta^{-/-}$ MSNs starting as early as 30 min after treatment, whereas at 60 min it was reduced by 71.5% (p < 0.0001) with respect to the initial signal for $Rar\beta^{-/-}$ and only non-significantly for WT MSNs (Fig. 2B). Analyses of the number of WT and $Rar\beta^{-/-}$ neurons as a function of Mitotracker intensity at 60 min after thapsigargin treatment revealed a bimodal distribution in both genotypes (Fig. 2E). Importantly, the very low-intensity population appeared in $Rar\beta^{-/-}$ cultures as major (10–40 AU) on expense of the group of high-intensity neurons (70 AU and more) which was strongly decreased, while the second population of intermediate-intensity neurons (50–60 AU) remained comparable between WT and $Rar\beta^{-/-}$ conditions. Such dynamics of distribution suggests existence of two neuronal populations with one of them being particularly prone to lose mitochondrial membrane potential in $Rar\beta^{-/-}$ cultures in response to thapsigargin treatment. In addition to decreased mitochondrial membrane potential, $Rar\beta^{-/-}$, but not WT MSNs displayed significant decrease (~59.2%) of the average volume of individual mitochondria per cell as measured at 60 min after treatment (Fig. 2C; p = 0.0016, unpaired t-test). The decrease in mitochondrial volume reflecting mitochondrial fragmentation and loss was associated with an increased cell death, as evidenced by a doubling of the number of pyknotic and fragmented nuclei in $Rar\beta^{-/-}$ cells (p = 0.0039, unpaired t-test) in comparison to WT cells (Fig. 2D).

3.3. Increased mitochondrial fragmentation and cell death of primary $Rar\beta^{-/-}$ striatal neuronal cultures in response to glutamate

Increased susceptibility to cell death related to abnormal calcium management and mitochondrial dysfunction in $Rar\beta^{-/-}$ cells may point to

neuroprotective activities of RARβ and suggest that compromised RARβ signalling may lead to increased sensitivity to glutamatergic excitotoxicity stress, a cause of cell death in a number of neurodegenerative diseases. We therefore challenged WT and $Rar\beta^{-/-}$ primary striatal neurons with glutamate (Fig. 3A), known to cause excitotoxicity in vivo and in vitro and contribute to HD progression. As expected, at 24 h after acute glutamate challenge there was a significant rise in cell death measured by lactate dehydrogenase (LDH) activity in WT cultures, but this increase was much stronger in $Rar\beta^{-/-}$ cells as indicated by significant interaction for treatment and genotype in two-way ANOVA ($F_{(1, 8)}$ = 48.08, p < 0.001) and Bonferroni post-hoc analyses (WT vs $Rar\beta^{-/-}$ glutamate treated cells, p < 0.0001) (Fig. 3B). At that time point glutamate-treated $Rar\beta^{-/-}$ cells, but not WT cells, displayed a significant increase in global amount of reactive oxygen species detected with CellROX, indicating enhanced oxidative stress (genotype x treatment interaction, $F_{(1, 16)}$ = 6.292, p < 0.05; vehicle vs glutamate for $Rar\beta^{-/-}$, p = 0.0206, Bonferroni post-hoc test; Fig. 3C). Analyses of MitoTracker signal intensity indicated that concomitant with exacerbated oxidative stress, mitochondrial membrane potential was also decreased (glutamate effect $F_{(1, 19)}$ = 45.82, p < 0.0001; Fig. 3D), and that this decrease was dependent on genotype (genotype x treatment interaction for MitoTracker intensity, $F_{(1, 19)}$ = 4.803, p < 0.05), reflecting stronger membrane depolarization in $Rar\beta^{-/-}$ than in WT neurons. Mitochondrial fragmentation was also affected by glutamate treatment in neurons based upon reduced MitoTracker volume (glutamate effect $F_{(1, 18)}$ = 35.26, p < 0.0001), but such reduction was comparable between WT and $Rar\beta^{-/-}$ cultures (Fig. 3 E).

Consistent with the cell death-promoting effects of the loss of RARβ function, pharmacological activation of RARβ using AC261066 led to
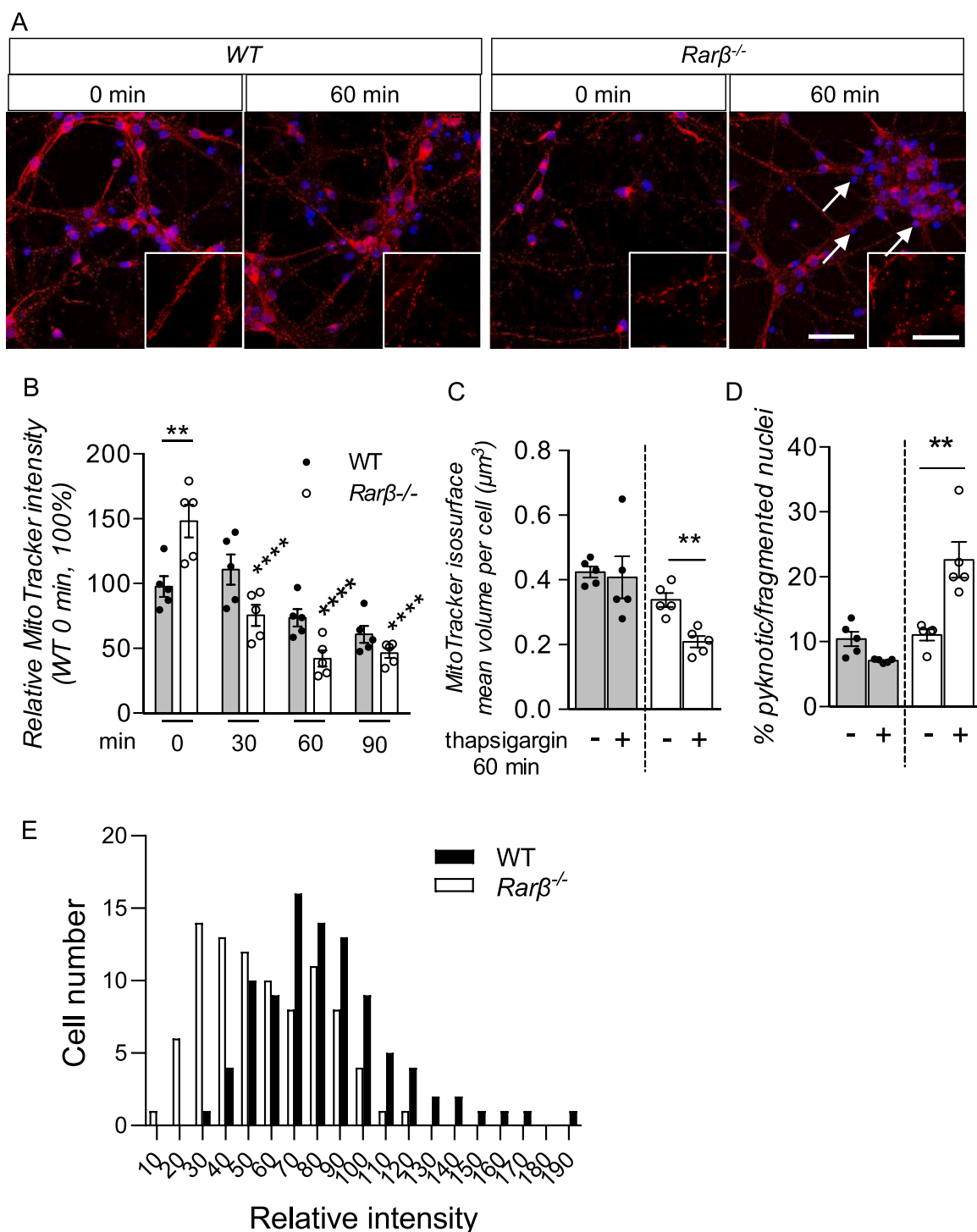
Fig. 2. Mitochondrial vulnerability and cell death of *Rarβ⁻/⁻* neurons in response to calcium overload. (A) Representative images of MitoTracker orange-stained mitochondria in WT and *Rarβ⁻/⁻* striatal cell cultures at 7 DIV, without treatment (0 min) or after a 60 min thapsigargin (1 μM) treatment. White arrows indicate examples of pyknotic nuclei. Scale bars: 30 μm for low and 10 μm for high magnification. (B) MitoTracker intensity indicative of mitochondrial membrane potential was quantified in WT and *Rarβ⁻/⁻* neurons at 0, 30, 60 and 90 min following thapsigargin treatment. (C) Mean mitochondrial volume indicated as MitoTracker isosurface, was quantified in WT and *Rarβ⁻/⁻* neurons at basal conditions and 60 min after thapsigargin treatment, and (D) pyknotic and fragmented nuclei were evaluated at the same time point (examples indicated with white arrows). (E) Frequency distribution of Mitotracker intensity in WT and *Rarβ⁻/⁻* neurons at 60 min after thapsigargin treatment. Scale bar in A = 50 μm for low and 10 μm for high magnification. Significant differences as compared to vehicle-treated WT samples are indicated: * ** *, $p < 0.0001$, * *, $p < 0.01$. Error bars represent SEM.

significant neuroprotective effects at the dose of 1 μM in WT cultures, whereas on its own (in absence of a challenging condition) this treatment did not significantly affect any of the measured parameters (Fig. 3A-E). Accordingly, glutamate-induced cell death in WT cells was

significantly reduced in the presence of AC261066 (AC261066 effect, $F_{(1, 8)} = 11.53$, $p < 0.01$) as illustrated by the significant decrease of the percentage of LDH release after glutamate treatment in AC261066 pre-treated cells in comparison with cells pre-treated with vehicle
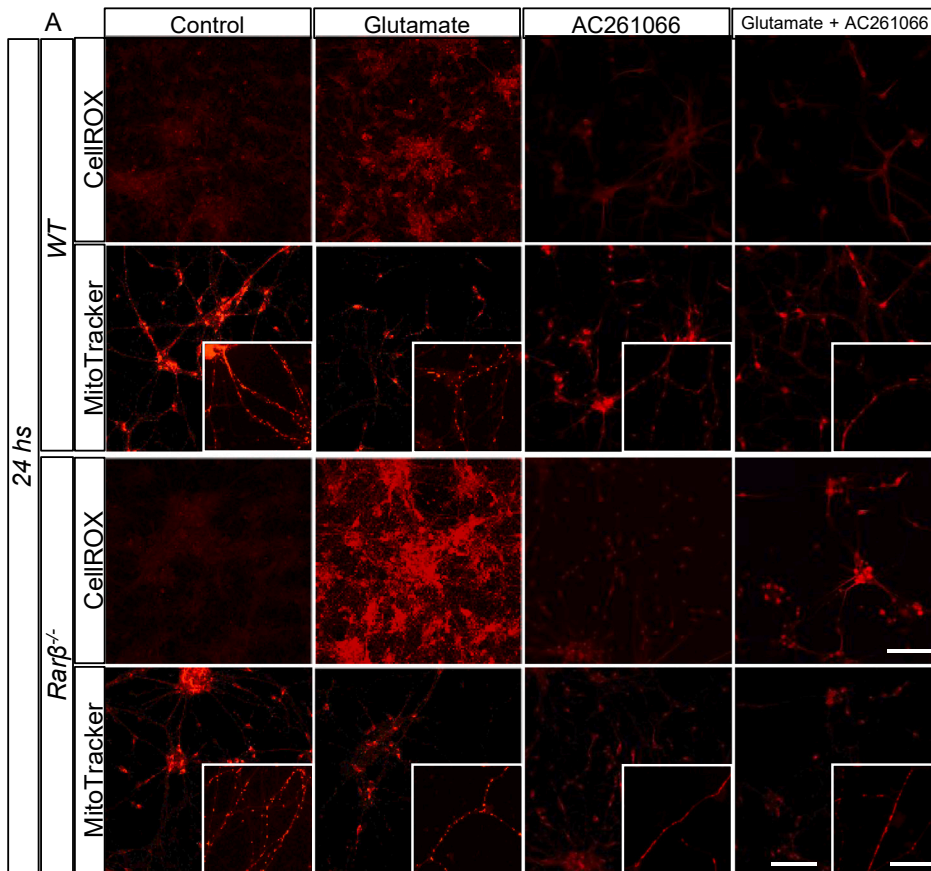
Fig. 3. RARβ control of mitochondrial vulnerability and cell death induced by glutamate excitotoxicity. (A) Representative images of CellROX and MitoTracker stained mitochondria in WT and *Rarβ*^{-/-} cultures as a function of 42 μM glutamate and/or 1 μM AC261066 treatments. Scale bars: 50 μm (CellROX) and 30 μm (MitoTracker) for low and 10 μm for high magnification. (B) LDH assay cytotoxicity data in WT and *Rarβ*^{-/-} cultures expressed as percentage of the WT glutamate-treated group. (C) Quantification of CellROX intensity staining analysis in WT and *Rarβ*^{-/-} cultures expressed as percentage of the WT vehicle-treated group. (D) Intensity of MitoTracker staining in WT and *Rarβ*^{-/-} cultures expressed as percentage of the WT vehicle-treated group. (E) Volume of individual, MitoTracker stained mitochondrial components per cell, in WT and *Rarβ*^{-/-} cultures was expressed as percentage of the WT vehicle-treated group. Statistical differences correspond to Bonferroni post-hoc analyses: *, p < 0.05; **, p < 0.01; ***, p < 0.001; ****, p < 0.0001. Error bars represent SEM.
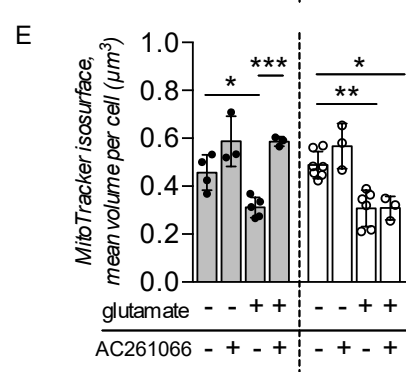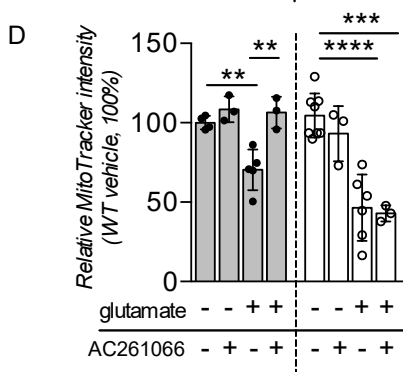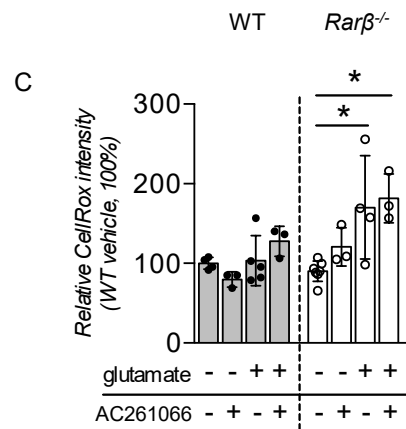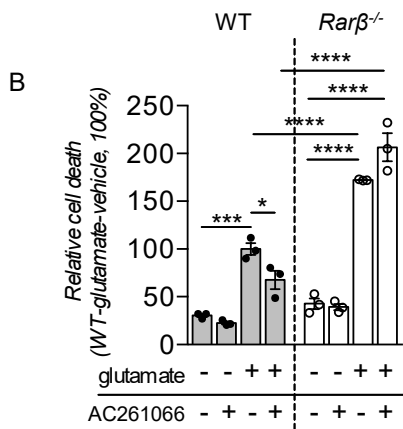
(Bonferroni post-hoc test, p = 0.0286; Fig. 3B). This protective effect was associated with AC261066-mediated prevention of mitochondrial injury by glutamate in WT cells, as evidenced by complete prevention of mitochondrial membrane depolarization (*glutamate x AC261066 interaction*, $F_{(1, 11)}$ = 7.096, p < 0.05; Bonferroni post-hoc test, p = 0.0022; Fig. 3D) and mitochondrial fragmentation (*glutamate x AC261066 interaction*, $F_{(1, 11)}$ = 4.47, p = 0.05; Bonferroni post-hoc test, p = 0.0007; Fig. 3E). Oxidative stress measures were not significantly affected in WT cells by glutamate or AC261066 treatments at this time point. The effect of AC261066 was RARβ-dependent, as AC261066 did not prevent oxidative stress, loss of mitochondrial potential, mitochondrial fragmentation or cell death in *Rarβ*⁻/⁻ cells treated with glutamate (Fig. 3A and graphs in 3B-E).

3.4. Rarβ loss leads to cell death and a reduced number of striatopallidal medium spiny neurons in knockout mice

To investigate whether the mitochondrial dysfunction and increased susceptibility to cell death observed in primary *Rarβ*⁻/⁻ MSN cultures may correlate with reduced striatal integrity *in vivo*, we analyzed cell death in the striatum of *Rarβ*⁻/⁻ mice. A subtle, but significant increase of the number of apoptotic cells was identified by activated caspase 3 immunofluorescence in the striatum of 8 weeks-old *Rarβ*⁻/⁻ mice (Fig. 4A, B). This discrete increase in cell death could lead in the long term to a significant decrease in cell number. To evaluate this possibility, we quantified the overall number of DAPI-positive cells throughout the striatum. We observed a significant ~25% reduction of DAPI-positive cells in the anterior, but not in the posterior part of the *Rarβ*⁻/⁻ striatum (Fig. 4C and S2A). Thus, focusing our analyses in the dorsal (caudate putamen; CPu) and ventral (nucleus accumbens; NAc) compartments of the anterior striatum, we asked whether cellular deficits are restricted to *Rarβ*-expressing cells, reflecting potential cell-autonomous activities of RARβ. To this end, we took advantage of the truncated non-functional *Rarβ* mRNA, which is still present in null-mutant mice (Ghyselinck et al., 1997) and allows to identify by *in situ* hybridization cells expressing *Rarβ* transcripts. Using a full-length *Rarβ* antisense riboprobe, we readily detected *Rarβ*-positive cells in WT and mutant mice (Fig. S2B), and observed that these cell numbers were significantly reduced, both in CPu (23%) and in NAc (22%) of the anterior striatum in mutant mice (Fig. S2C and Table S1 for examples and exact counts). To assess the identity of affected cell population(s), we performed a series of *in situ* hybridization analyses with cell-type specific probes. A ~27% decrease of GAD67-positive GABAergic MSNs, both in dorsal part of CPu and in NAc (Fig. 4D, E, Table S1), could account for most (if not all) cellular deficits. Furthermore, in agreement with a previous report on compromised development of striatonigral MSNs in *Rarβ*⁻/⁻ striatum (Rataj-Baniowska et al., 2015), we observed a significant reduction in the number of MSNs expressing striatonigral-specific markers, including *Drd1* (19% and 16% reduction in *Rarβ*⁻/⁻ CPu and NAc, respectively) and *Tac1* (40% and 27% reduction in *Rarβ*⁻/⁻ CPu and NAc) (Fig. 4D, F, G, Table S1). This reduction was comparable to 23 ± 8.4% decrease of *Drd1*-expressing neurons scored in newborn (P0) *Rarβ*⁻/⁻ mice (Rataj-Baniowska et al., 2015), indicating that no further reduction of Drd1 + neurons appeared in post-natal life. Unexpectedly, we also found a significant deficit in the number of striatopallidal MSNs expressing *Drd2* (about 25% in the CPu and NAc) and proenkephalin (*pENK*; 25% and 14% reduction in *Rarβ*⁻/⁻ CPu and NAc; Fig. 4D, H, I and Table S1). Since striatopallidal neurons are not affected prenatally at E18.5 and at birth in *Rarβ*⁻/⁻ striatum (104.2 ± 4.5% of WT *Drd2* + MSNs and no change in mRNA level quantified by qPCR) (Rataj-Baniowska et al., 2015), the present findings indicate that such a deficit appears in postnatal life and may result from neurodegeneration, as supported by the increase in caspase 3 immunoreactivity. The Drd2-type specificity of cell loss in the adult *Rarβ*⁻/⁻ striatum cannot be explained by preferential expression of RARβ in this cell population, as in WT striatum similar percentages of *Drd1* + and

Drd2 + cells expressed *Rarβ* (82 ± 3.7% and 76 ± 3.5% respectively; Fig. S3 A, B, D), whereas *Drd1* + represented 43 ± 3% and *Drd2* + 46 ± 2% of *Rarβ* cells (Fig. S3 A, B, E).

Considering that striatonigral and striatopallidal MSNs are inhibitory GABAergic neurons, an overall, about 20% deficit of each individual population of Drd1 + and Drd2 + neurons was unexpectedly high comparing to the 27% reduction of GAD67 neurons in corresponding regions. We therefore explored the possibility that reduced number of MSNs co-expressing both dopaminergic receptors may explain such difference. Using double fluorescent *in situ* hybridization for *Drd1* and *Drd2,* we confirmed that this cellular population represents about 5% of all cells in the dorsal CPu and 15% in the NAc of WT mice, which agrees with data obtained using BAC reporter lines (Valjent et al., 2009). Importantly, the number of *Drd1-Drd2* co-expressing cells was reduced by about 40% in both the dorsal CPu and NAc in mutants (Fig. S3C, F). Thus, high cumulative deficit of *Drd1* + and *Drd2* + cells as compared to more moderate decrease of GAD67 + cells can be at partially accounted for by strong decrease of cells expressing both of those markers.

3.5. Functional deficits of the striatopallidal pathway in Rarβ⁻/⁻ mice

Reduced number of *Drd1* and *Drd2* expressing cells may suggest unbalanced striatonigral *vs* striatopallidal pathway signalling in the striatum of *Rarβ*⁻/⁻ mice. To functionally dissect signalling through each pathway, we used a pharmacological approach by modulating dopamine signaling by amphetamine or challenging *Rarβ*⁻/⁻ mice with Drd1- or Drd2-selective ligands and monitoring behavioral and molecular outputs. Enhancement of dopaminergic signalling following acute amphetamine treatment induced a marked increase of locomotor activity in WT mice, which attained its maximum at 30 min after injection (Fig. 5A). Such increase was significantly blunted in *Rarβ*⁻/⁻ mice as revealed by significant interaction for *genotype x treatment* for an overall horizontal motor activity ($F_{(1.24)}$= 6.51, p < 0.05; two-way ANOVA on repeated measures) and best illustrated for the first 60 min following amphetamine injection, when *Rarβ*⁻/⁻ mice scored overall 253.2 ± 52.6 beam breaks as compared to 552.8 ± 90.3 for WT animals (p < 0.001; unpaired student t-test). Such data may reflect compromised dopaminergic signalling through Drd2, as a similar decrease of reactivity was observed in *Drd2*⁻/⁻ mice (Baik et al., 1995; Kelly et al., 2008), but not *Drd1*⁻/⁻ mice (Karper et al., 2002; McDougall et al., 2005; Xu et al., 2000). To further address function of the indirect pathway we used haloperidol, a Drd2 preferential antagonist, which at the dose of 1 mg/kg induced catalepsy in WT mice, whereas such activity was strongly blunted in *Rarβ*⁻/⁻ mice (Fig. 5B). In support of compromised activation of the striatopallidal pathway, the number of haloperidol-induced cFos-positive cells was significantly lower (~50%) in *Rarβ*⁻/⁻ striatum (p < 0.001; unpaired student t-test) (Fig. 5C, D). Such a severe deficit reflects most probably a dysfunction of remaining *Drd2* + spMSNs, as cell loss was observed only for ~20% of *Drd2* + cells in *Rarβ*⁻/⁻ striatum.

To assess the function of the direct pathway, we used SKF 81297, a selective D1-like receptor agonist. After the habituation period of 60 min, SKF 81297 (4 mg/kg) was administered to the animals and locomotor activity was monitored for 1 h. Comparing to vehicle (saline)-injected mice (95.7 ± 41.8 beam breaks in WT and 89.8 ± 24.5 beam breaks in *Rarβ*⁻/⁻ mice), SKF 81297 similarly increased locomotion in WT and *Rarβ*⁻/⁻ mice (141 ± 23.1 and 120.3 ± 25.8 beam breaks, respectively) (Fig. 5E). Moreover, the number of cFos-expressing cells induced after SKF 81297 administration was similar in both genotypes (97.1 ± 5.7 cells/mm² in *Rarβ*⁻/⁻ mice *vs* 94.3 ± 4.0 cells/mm² in WT) (Fig. 5F).

3.6. Behavioral consequences of unbalanced direct (striatonigral) versus indirect (striatopallidal) pathway signaling in Rarβ⁻/⁻ mice
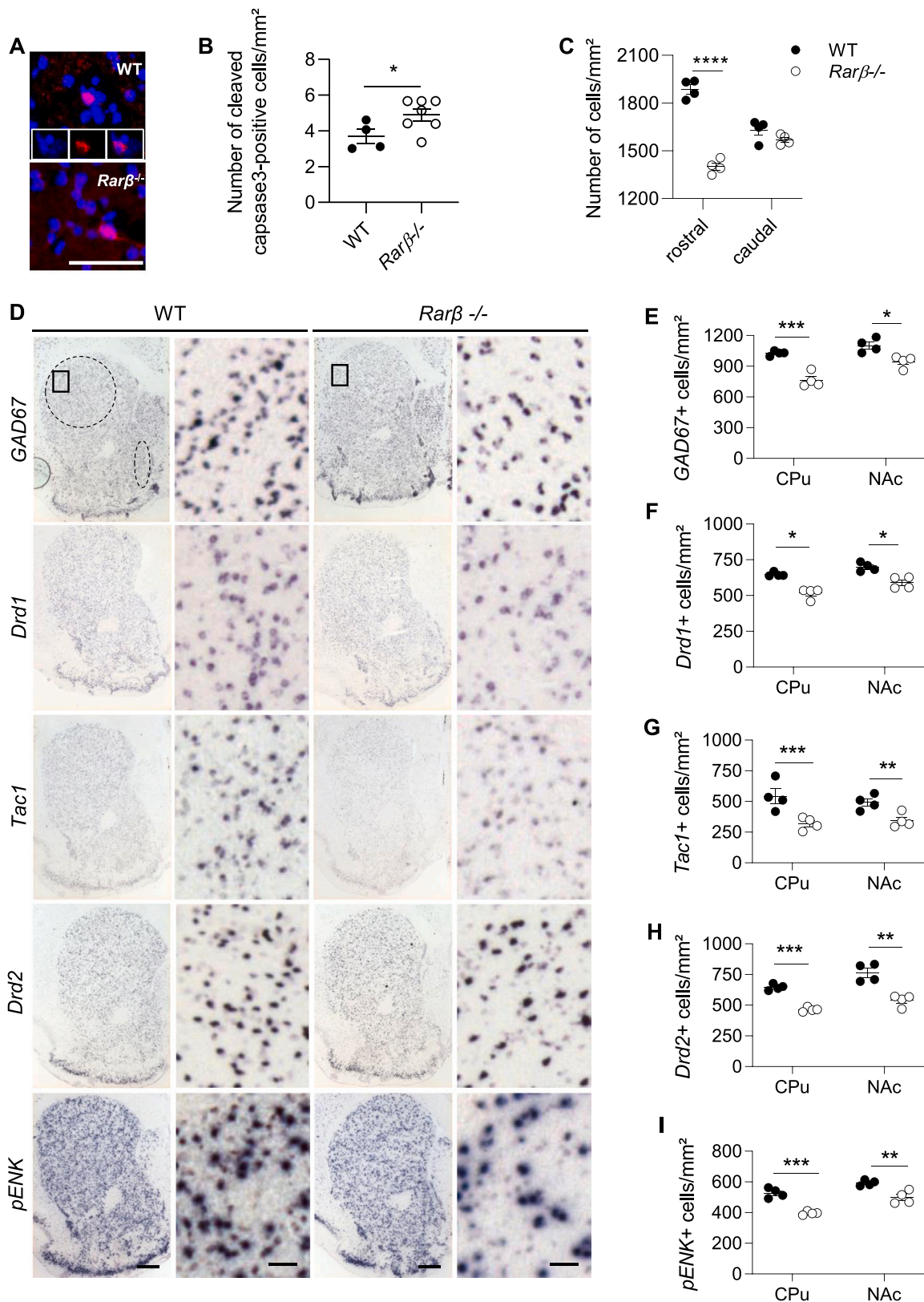
Considering that dopaminergic signaling through D1 and D2

Fig. 4. Cell loss in *Rarβ⁻/⁻* striatum. (A) Activated caspase 3 (red) was detected by immunofluorescence in WT and *Rarβ⁻/⁻* striatum of 8 weeks-old mice and (B) scored when colocalized with nuclear DAPI staining (blue) in CPu region. (C) Total counts of DAPI-positive cells in the dorsolateral region of CPu in WT and *Rarβ⁻/⁻* striatum. (D) Examples of *in situ* hybridization identification of *GAD67*-positive neurons and snMSNs (*Drd1, Tac1*) or spMSNs (*Drd2, pENK*). Selected regions of dorsolateral striatum (see rectangles) were enlarged in adjacent panels and correspond to the areas used for scoring number of cells positive for (E) *GAD67*, (F) *Drd1*, (G) *Tac1*, (H) *Drd2*, (I) *pENK*. Scale bars: 200 μm (A), 500 μm (D, low magnification), 20 μm (D, high magnification). Statistical differences were calculated using unpaired t-test and indicate: * , $p < 0.05$, * * , $p < 0.01$, * ** , $p < 0.001$. Error bars represent SEM.
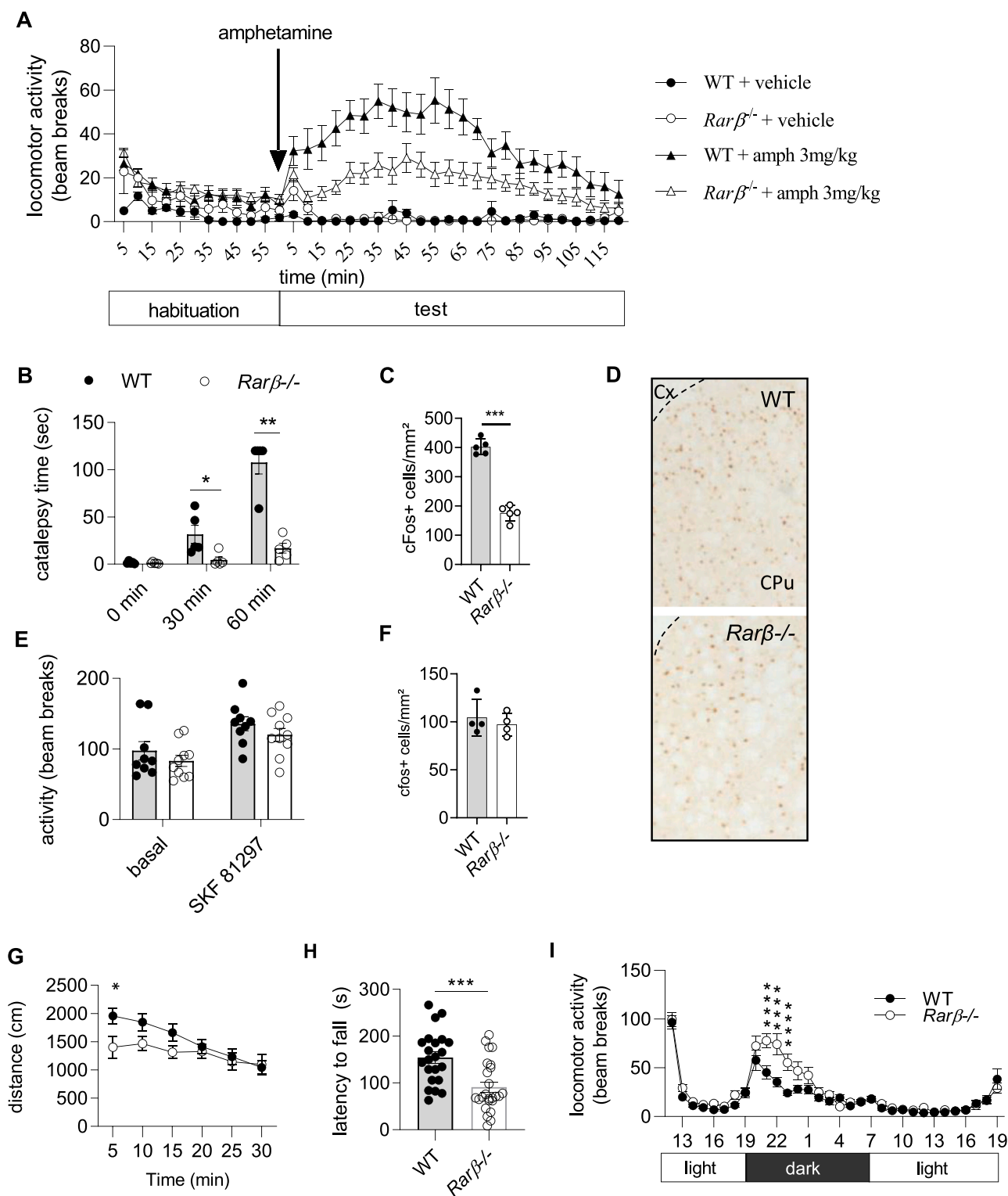
Fig. 5. Compromised signalling of striatopallidal pathway and behavioral deficits in *Rarβ⁻/⁻* mice. (A) Amphetamine (3 mg/kg)-induced locomotor activity was evaluated over 120 min in actimetric cages after a 60 min habituation period for n = 6 WT and n = 10 *Rarβ⁻/⁻* 12-weeks old mice. (B) Catalepsy evaluated as latency to move in the bar-test was measured before and after haloperidol (1 mg/kg) treatment in n = 5 WT and n = 5 *Rarβ⁻/⁻* mice, which were next used for (C) evaluation of haloperidol-induced cFos expression in the dorsolateral CPu at 90 min after treatment. (D) Representative example of immunodetection of cFos expression in the striatum. (E) Drd1 agonist-induced activity was scored in actimetric cages prior to (basal) and after SKF81297 (4 mg/kg) treatment. (F) The number of cFos-positive cells was quantified in dorsolateral striatum at 90 min following SKF 81297 treatment. (G) Novelty induced locomotor activity in the open field for n = 10 WT and n = 10 *Rarβ⁻/⁻* mice. (H) Motor coordination was evaluated in accelerated rotarod as mean latency to fall from the rotating cylinder. (I) Spontaneous locomotor activity was measured in actimetric cages over 32 h in n = 20 WT and n = 23 *Rarβ⁻/⁻* 14–16 week old mice. Statistical differences were calculated using Bonferroni multiple comparisons as post-hoc follow-up of ANOVA analyses or unpaired t-test and indicate as indicated in the text: *, $p < 0.05$; **, $p < 0.01$; ***, $p < 0.001$; ****, $p < 0.0001$. Error bars represent SEM.

receptors is critically involved in the control of motor behaviors, we tested locomotor performance *Rarβ⁻/⁻* and WT mice in several behavioral paradigms. Novelty-induced locomotion in an open field evolved differently in *Rarβ⁻/⁻* mice as compared to WT group (F$_{(5,90)}$= 2.916,

p = 0.0174 for *genotype x time* interaction in one-way ANOVA), which reflected a significant reduction of activity in *Rarβ⁻/⁻* mice during the first 15 min of the task (Fig. 5G). This reduction reflects motor deficits, as *Rarβ⁻/⁻* mice also displayed a significant reduction of motor
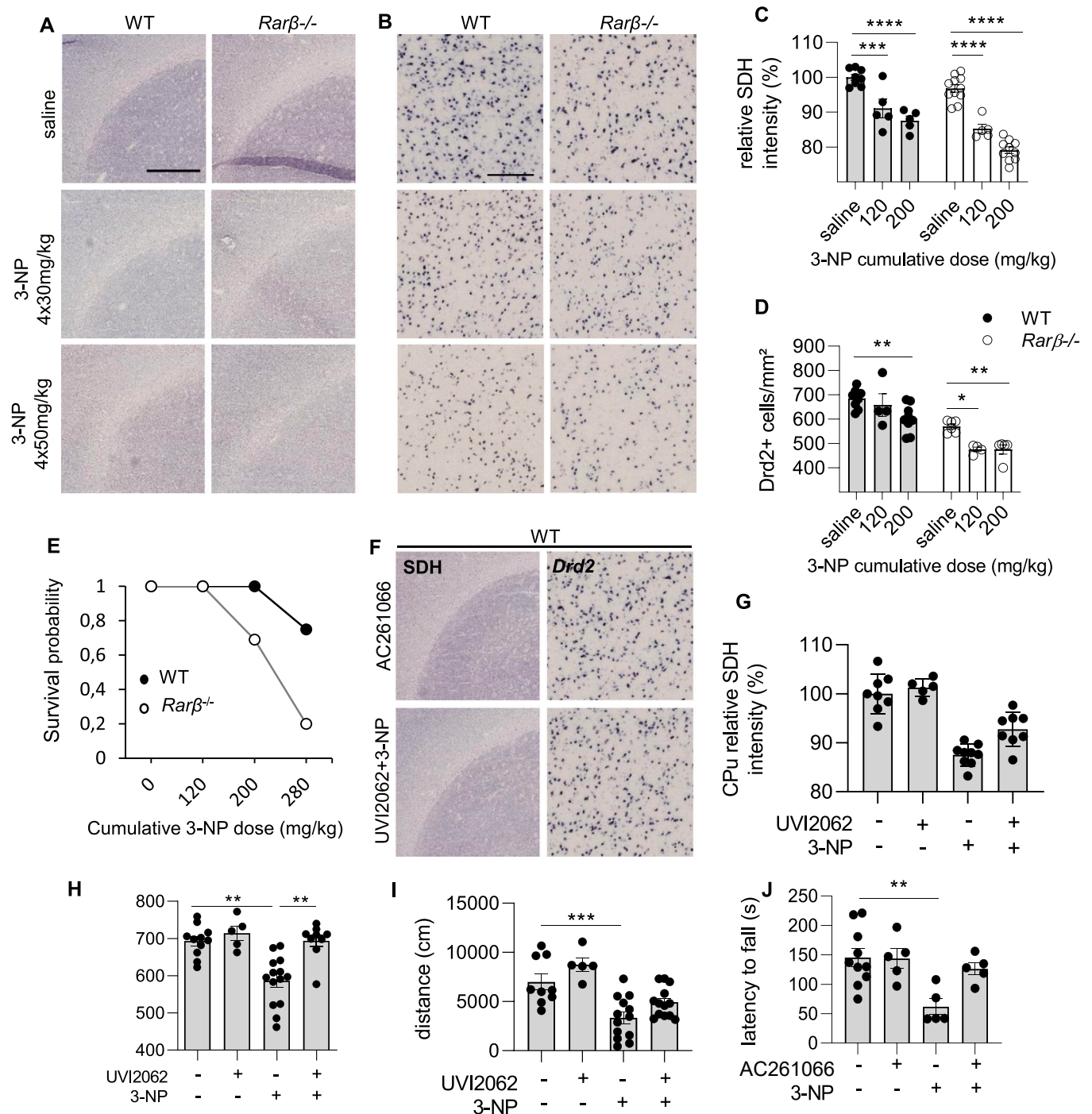

Fig. 6. Neuroprotective activity of RARβ *in vivo* involves mitochondrial functions. (A) Representative images of histochemical detection of SDH activity in cry-osections from WT and *Rarβ⁻/⁻* striatum after saline or 3-NP treatment. (B) Examples of *Drd2* detection by *in situ* hybridization in 12-weeks old WT and *Rarβ⁻/⁻* striatum after saline or 3-NP treatment. (C) Effects of 3-NP treatments on relative SDH activity in the dorsolateral striatum were expressed as percent of mean value of WT vehicle-treated group. (D) Scores of *Drd2*-positive neurons detected by *in situ* hybridization in the dorsolateral striatum. (E) Survival probability in WT and *Rarβ⁻/⁻* mice was evaluated as function of the 3-NP dose (for details see also Table S2). (F) Images of detection of SDH enzymatic activity (left column) and *Drd2*-expressing neurons (*in situ* hybridization; right column) in the dorsolateral striatum from WT mice following AC261066 or AC261066 and 3-NP treatments. (G) Quantification of SDH enzymatic activity and (H) *Drd2*-positive cell number as a function of AC261066 (2 mg/kg) and/or 3-NP (200 mg/kg) treatment. (I) Locomotor activity in the open field and (J) motor coordination on the rotarod evaluated on the second day of AC261066 and/or 3-NP treatment. Scale bars, 500 μm (low magnification) and 200 μm (high magnification). Statistical differences were calculated using Bonferroni multiple comparisons as post-hoc follow-up of ANOVA analyses or unpaired t-test and indicate as indicated in the text: *, p < 0.05; **, p < 0.01; ***, p < 0.001; ****, p < 0.0001. Error bars represent SEM.

coordination in the rotarod test, as seen with a shorter latency to fall from the accelerating cylinder (Fig. 5H). These measures were not confused by altered reactivity to stress, as anxiety-related measures, including percent of time spent in the center of the open field during the first 5 min of the test (7.53 ± 2.67% for $Rar\beta^{-/-}$ mice and 8.58 ± 1.73 for WT) and percent of time spent in the open arms of the elevated plus maze (12.11 ± 1.23% for $Rar\beta^{-/-}$ mice and 17.33 ± 3.61% for WT), were not affected by RARβ loss of function (Fig. S4 A, B). In contrast to reduced motor performance in the open field and rotarod tests, $Rar\beta^{-/-}$ mice displayed a significant increase in their spontaneous horizontal activity in actimetric cages, as supported by an effect of *genotype* ($F_{(1,41)}$ = 6.211, p = 0.0168) and significant interaction *genotype x time* ($F_{(31,1271)}$ = 3.341, p < 0.0001, one-way ANOVA on repeated measures). This increase of activity was apparent only during the active, dark phase of the light/dark cycle (Fig. 5I).

3.7. An RARβ agonist prevents mitochondrial dysfunction and neurodegeneration in the 3-NP mouse model of HD

Administration of 3-nitropropionic acid (3-NP), an inhibitor of mitochondrial SDH / complex II activity, was previously demonstrated to cause selective striatal degeneration with loss of MSNs and HD-like deficits in rodents and non-human primates (Blum et al., 2003; Ludolph et al., 1991; Page et al., 2000; Sun et al., 2002), and thereafter was extensively used as pharmacological model of HD-like symptoms (Brouillet et al., 2005). To further test the functional relevance of compromised mitochondrial and SDH activity in $Rar\beta^{-/-}$ striatum and investigate the neuroprotective activities of RARβ, we studied the effects of loss or gain of RARβ function on mouse behavior, mitochondrial SDH activity, and MSN cell survival in mice treated with 3-NP. We observed dose-dependent effects of 3-NP on striatal SDH activity *in situ* (Fig. 6A, C) and loss of *Drd2*+ neurons (Fig. 6B, D), but not *Drd1*+ neurons (Fig. S5), in both WT and $Rar\beta^{-/-}$ mice. Importantly, whereas a low, cumulative dose of 120 mg/kg of 3-NP (4 treatments with 30 mg/kg, see materials and methods) induced a significant reduction of SDH activity in both WT and $Rar\beta^{-/-}$ striatum (Fig. 6C), only $Rar\beta^{-/-}$ mice displayed significant reduction of the number of *Drd2*+ neurons (effect of 120 mg/kg 3-NP treatment $F_{(1,19)}$ = 8.579, p < 0.05 in two-way ANOVA; p > 0.9, not significant, for WT-saline *vs* WT-120 mg/kg and p < 0.05 for $Rar\beta^{-/-}$-saline *vs* $Rar\beta^{-/-}$-120 mg/kg, post-hoc Bonferroni test). Furthermore, higher doses of 3-NP were associated with mortality in ~ 25% of $Rar\beta^{-/-}$ mice only for 200 mg/kg, and 80% of $Rar\beta^{-/-}$ and 25% of WT mice for 280 mg/kg (Fig. 6E and Table S2), supporting increased vulnerability of $Rar\beta^{-/-}$ mice to the mitochondrial toxin. Such increased mortality of $Rar\beta^{-/-}$ mice likely accounts for comparable scores of SDH activity and *Drd2*+ cell number for 200 mg/kg 3-NP in WT and surviving $Rar\beta^{-/-}$ mice (Fig. 6C, D).

Taking advantage of the 3-NP model, we asked whether gain of RARβ function following AC261066 agonist treatment can prevent adverse effects of 3-NP (200 mg/kg) in WT mice. Thus, whereas 3-NP treatment strongly reduced SDH activity, such effect was dampened in mice which received 2 mg/kg of AC261066 prior to 3-NP treatment (Fig. 6G, compare also panel A with SDH in F), which was not different from vehicle-treated group (3-NP treatment effect $F_{(1,26)}$ = 81.46, p < 0.0001, AC261066 treatment effect $F_{(1,26)}$ = 7.79, p = 0.0097 in 2-way ANOVA; p < 0.01 for saline *vs* 3-NP and p = 0.07 for saline *vs* AC261066 + 3-NP, post-hoc Bonferroni test), and was significantly weaker than in 3-NP treated group (p < 0.05 for 3-NP+AC261066 *vs* 3-NP, post-hoc Bonferroni test). Importantly, AC261066 prevented loss of *Drd2*+ spMSNs (Fig. 6H, compare also panel B with *Drd2* in F) in 3-NP+AC261066-treated WT mice (3-NP treatment effect $F_{(1,36)}$ = 31.42, p < 0.0001, AC261066 treatment effect $F_{(1,36)}$ = 6.284, p < 0.05 in 2-way ANOVA; p < 0.01 for saline *vs* 3-NP and p < 0.01 for 3-NP *vs* AC261066 + 3-NP, post-hoc Bonferroni test). The same dose of AC261066 alone (in absence of 3-NP treatment) did not affect SDH or *Drd2*+ cell counts (Fig. 6G, H, compare also top rows of panel A and B

with F). In addition, behavioral evaluation of novelty-induced locomotor activity (Fig. 6I) and motor coordination (Fig. 6J) on the second day of 3-NP treatment point to partial prevention of behavioral deficits during treatment. Distance covered by 3-NP-treated mice in the open field test was significantly lower than for control, saline-treated animals (3-NP treatment effect $F_{(1,36)}$ = 31.42, p < 0.0001 in two-way ANOVA; p < 0.001 for saline *vs* 3-NP, Bonferroni test), but such difference became insignificant in 3-NP group pretreated with AC261066 (p = 0.1, not significant, for saline *vs* 3-NP+AC261066 comparison, Bonferroni test). Similarly, 3-NP-treated mice displayed significant reduction of latency to fall from the rotating cylinder in rotarod test indicating a locomotor coordination deficit, which was prevented by AC261066 pretreatment (3-NP treatment effect $F_{(1,21)}$ = 9.423, p < 0.01 in two way ANOVA; p < 0.01 for saline *vs* 3-NP comparison and p > 0.9 for saline *vs* 3-NP+AC261066, not significant, Bonferroni test).

3.8. AAV-mediated inactivation of RARβ in the adult striatum leads to progressive motor deficits and loss of spMSNs

Deficits of *Drd2* + spMSNs in adult, but not in newborn $Rar\beta^{-/-}$ mice, and possibility of preventing spMSN cell loss by administering a RARβ agonist in 3-NP-treated WT mice suggest postnatal neuroprotective activity of RARβ in these cells. To address this possibility and exclude neurodevelopmental origin of vulnerability of spMSNs in $Rar\beta^{-/-}$ mice, we investigated the effects of a postnatal inactivation of RARβ following AAV9-mediated expression of an EGFPCre fusion protein in the striatum of mice carrying floxed $Rar\beta$ alleles. Efficiency of bilateral viral infection and RARβ inactivation in the striatum of $Rar\beta^{AAV9EGFPCre}$ mice was verified post-hoc by immunofluorescent analyses and compared to a control group of floxed $Rar\beta$ mice injected with AAV9EGFP virus (Fig. 7A). RARβ was undetectable in cells expressing AAV9EGFPCre in $Rar\beta^{AAV9EGFPCre}$ mice (Fig. 7A, bottom panels). In control mice, all cells expressing EGFP also expressed RARβ (Fig. 7A, upper panels). Western blot analyses revealed ~94% reduction of RARβ expression in the striatum (Fig. 5B, C). Longitudinal monitoring of locomotor coordination and spontaneous activity (two behavioral tests used here as sensitive, key readouts associated with RARβ inactivation) revealed progressive motor abnormalities in mice with conditional inactivation of RARβ. Accordingly, whereas control $Rar\beta^{AAV9EGFP}$ mice gradually improved their locomotor coordination over successive testing sessions on the rotarod, $Rar\beta^{AAV9EGFPCre}$ did not display such motor learning and their performance showed opposite deteriorating tendency supported by significant *genotype x time* interaction ($F_{(3,45)}$ = 8.9 in two-way ANOV, p < 0.001; Fig. 7D). Consequently, their performance was reduced by 43% at 20 weeks after viral infection as compared to control $Rar\beta^{AAV9EGFP}$ mice (p < 0.05; post-hoc Bonferroni test). Inactivation of RARβ also led to progressive increase of spontaneous motor activity during active, dark phase of the light/dark cycle, which was not observed in control mice as indicated by significant *genotype x time* interaction ($F_{(3,45)}$ = 2.8 in two-way ANOVA, p < 0.05; Fig. 7E and Fig. S6 A-D). Also, motor reactivity to manipulation and novelty progressively increased following ablation of RARβ as indicated by significant increase in the activity of $Rar\beta^{AAV9EGFPCre}$ mice during the first hour of testing in actimetric cages at 10 and 20 weeks after viral injection when compared to control $Rar\beta^{AAV9EGFP}$ mice, as supported by significant interaction of *genotype x time* ($F_{(3,45)}$ = 4.3, p < 0.01) (Fig. S6 E). *In situ* hybridization detection and quantification of striatal MSNs at 21 weeks after viral injection revealed significant reduction of about 12% of *GAD67* + MSNs which may reflect loss of about 15% of *Drd2* + spMSNs but not *Drd1* + snMSNs in the striatum of $Rar\beta^{AAV9EGFPCre}$ mice when compared to control $Rar\beta^{AAV9EGFP}$ mice (Fig. 7F).
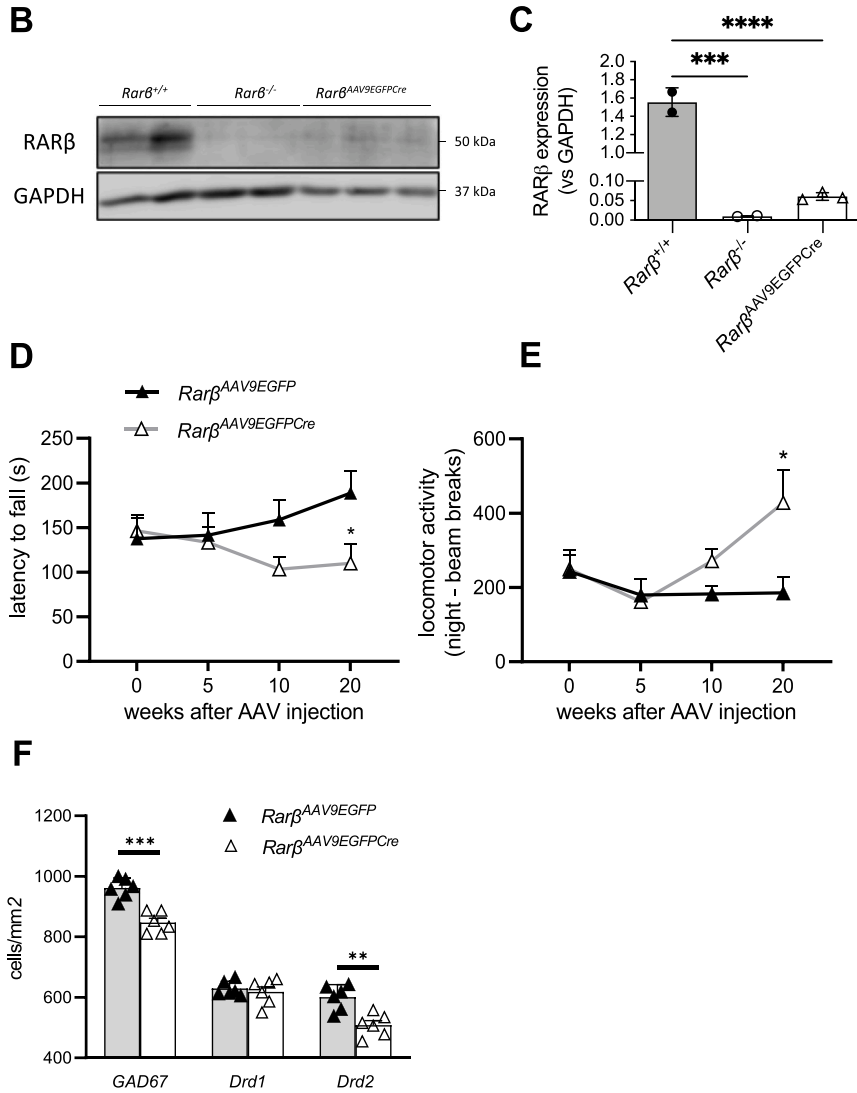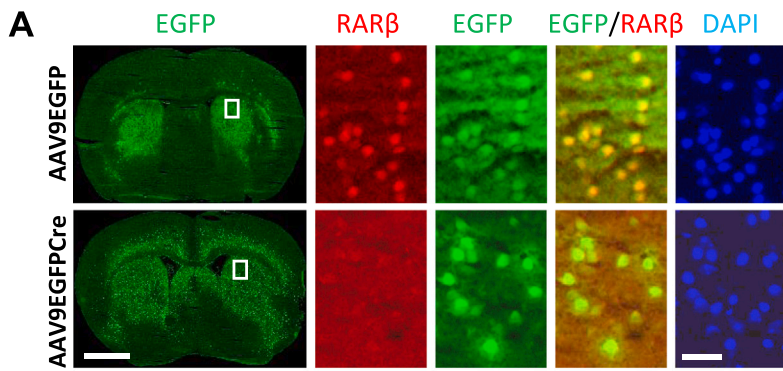
Fig. 7. Conditional striatal inactivation of RARβ in adult mice. (A) Examples of bilateral expression of EGFP illustrating viral infection in the striatum (low magnification images, top and bottom left). RARβ expression was detected in the striatum of *Rarβ* floxed mice infected with control AAV9EGFP virus (top panel) corresponding to control *Rarβ^AAV9EGFP* cohort, whereas it was absent following conditional ablation of RARβ following AAV9EGFPCre virus infection in *Rarβ^AAV9EGFPCre* mice (bottom panel). (B) Western blot detection of RARβ and its quantification (C) in WT, *Rarβ^-/-* and *Rarβ^AAV9EGFPCre* striatum. Longitudinal behavioral analyses were performed for n = 8 *Rarβ^AAV9EGFP* and n = 9 *Rarβ^AAV9EGFPCre* mice which displayed efficient bilateral viral infection. This included (D) monitoring of locomotor coordination and (E) spontaneous locomotor activity during active, dark phase of the light/dark cycle prior to viral infection (week 0) and at 5, 10 and 20 weeks after virus injection. (F) *GAD67 +*, *Drd1 +* and *Drd2 +* cells were detected using *in situ* hybridisation and counted in dorsal striatum of n = 6 mice/group. Scale bars in A: 2 mm (low magnification images, left panels) and 20 μm (high magnification panels). Statistical differences were shown in comparison to *Rarβ^AAV9EGFP* mice for corresponding time-points using Bonferroni multiple comparisons as post-hoc follow-up of ANOVA analyses or unpaired t-test and indicate as indicated in the text: *, p < 0.05, **, p < 0.01, ***, p < 0.001. Error bars represent SEM.

3.9. Inactivation of RARβ in Drd2 + spMSNs leads to selective decrease of spMSN number and function and partially recapitulates Rarβ^-/- motor phenotype

Whereas germline together with postnatal AAV-mediated deletion of RARβ pointed to postnatal role of RARβ in neuroprotection and functions of spMSNs, it is not clear, if such effects are cell autonomous, and what is specific contribution of RARβ-dependent functions in spMSN to an overall behavioural abnormalities observed in *Rarβ^-/-* mice. To address these questions, we have deleted *Rarβ* in post-mitotic spMSNs by transgenic expression of Drd2-Cre in mice carrying floxed *Rarβ* alleles. As expected from the distribution of *Rarβ* expression within *Drd1 +* and *Drd2 +* MSNs (note that ~40% of *Rarβ+* cells express *Drd2*; Fig. S3) the number of RARβ+ cells was reduced by ~40% in *Rarβ^Drd2-/-* mice as compared to *Rarβ^Drd2+/+* control mice (Fig. 8A-B). The 8-weeks old *Rarβ^Drd2-/-* mice displayed reduction of an overall motor activity in the open field as indicated by significant effect of genotype ($F_{(1,16)} = 5.2$, p < 0.05 and post-hoc analyses for the initial 10 min, p < 0.05; Fig. 8C).
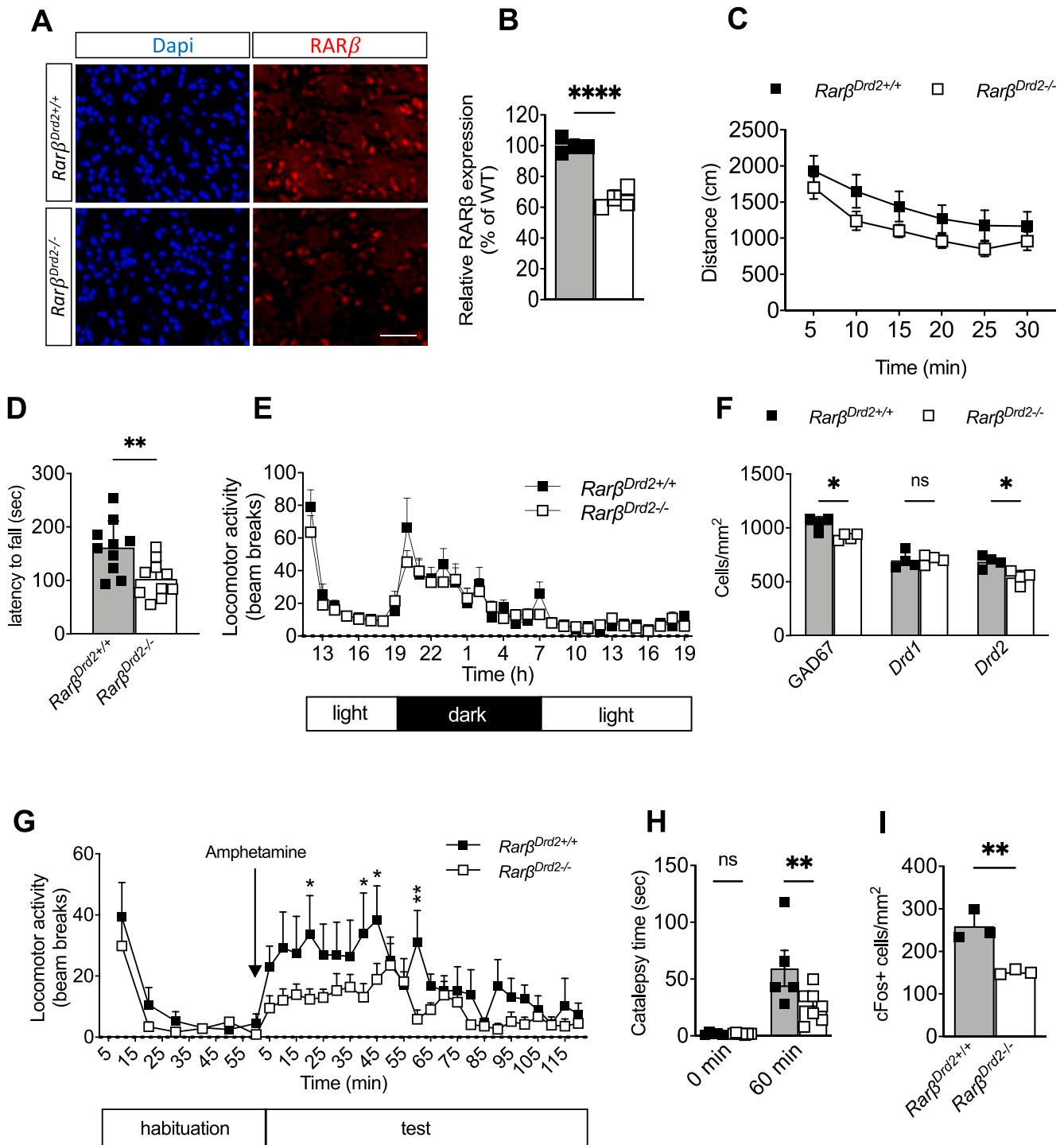
Fig. 8. Somatic deletion of RARβ in post-mitotic Drd2 + neurons. (A) Examples of immunodetection of RARβ+ cells and (B) their quantification in control, *Rarβ*^Drd2+/+^ and *Rarβ*^Drd2-/-^ mice. Behavioral analyses were performed on *Rarβ*^Drd2+/+^ and *Rarβ*^Drd2-/-^ mice (n = 10/genotype) mice at the age of 8 weeks and included (C) analyses of novelty induced motor activity in the open filed, (D) monitoring of locomotor coordination on the rotarod and (E) spontaneous locomotor activity during light/dark cycle. (F) *GAD67* + , *Drd1* + and *Drd2* + cells were detected using *in situ* hybridisation and counted in dorsal striatum of n = 4 mice/group. (G) Amphetamine (3 mg/kg)-induced locomotor activity was scored over 120 min in actimetric cages after a 60 min habituation period. (B) Catalepsy in the bar-test was measured before and 60 min after haloperidol (1 mg/kg) treatment in n = 5 *Rarβ*^Drd2+/+^ and n = 7 *Rarβ*^Drd2-/-^ mice mice. (C) In 3 randomly selected mice/genotype cFos expression was quantified at 90 min after haloperidol treatment. Scale bar in A, 10 μm. Statistical differences were shown in comparison to *Rarβ*^Drd2+/+^ mice and calculated using unpaired t-test or Bonferroni test as a post-hoc analyses of ANOVA measures: * , p < 0.05, * *, p < 0.01. Error bars represent SEM.

Similarly, to *Rarβ*^-/-^ mice, locomotor coordination was compromised in *Rarβ*^Drd2-/-^ mutants on evidence of significant ~30% decrease of latency to fall from the rotarod (Fig. 8D). Intriguingly, unlike for germline or somatic striatal deletion of RARβ in *Rarβ*^-/-^ in *Rarβ*^AAV9EGFPCre^ mice we did not observe any spontaneous hyperactivity in the actimetric cages

during dark phase of the light/dark cycle (Fig. 8E), suggesting that abnormal activity of snMSNs *Rarβ*^-/-^ in *Rarβ*^AAV9EGFPCre^ mice contributes to this hyperactivity phenotype or alternatively that spMSN pathway signalling is only weakly impacted in *Rarβ*^Drd2-/-^ mice. To address this latter possibility, we evaluated MSNs numbers and functions with

particular focus on spMSNs. Cell number analyses carried out at 11 weeks of age revealed significant, 10% reduction of *GAD67* + MSNs which may reflect loss of about 16% of *Drd2* + spMSNs, but not *Drd1* + snMSNs in the striatum of *Rarβ*[Drd2-/-] mice (Fig. 8F). Furthermore, locomotor response to amphetamine stimulation was reduced by about 50% in *Rarβ*[Drd2-/-] animals (effect of *genotype* $F_{(1540)} = 27.3$, p < 0.05; and post-hoc analyses shown in Fig. 8G) which was similar to reduction observed in *Rarβ*^{-/-} mice (compare with Fig. 5A). Challenging DRD2 receptors with 1 mg/kg haloperidol resulted in catalepsy, which was significantly reduced in *Rarβ*[Drd2-/-] mice (Fig. 8H) and accompanied by significant, decrease of the number of cells in which cFos expression was activated (Fig. 8I). Similarly to what was observed in *Rarβ*^{-/-} mice, about ~50% reduction in haloperidol-induced cFos expression exceeded largely reduction of 16% *Drd2* + cell number indicating that in addition to neuroprotection, RARβ most probably modulates /downregulates activity of existing spMSNs. Furthermore, absence of spontaneous hyperactivity in *Rarβ*[Drd2-/-] despite comparable deficit in spMSN number and function in *Rarβ*[Drd2-/-], *Rarβ*^{-/-} and/or *Rarβ*[AAV9EGFPCre] mice indicates that such hyperactivity phenotype reflects most probably abnormal functions of remaining snMSNs.

4. Discussion

HD is characterized by a wide range of transcriptional changes which are globally similar between HD patients and respective animal models. Recent analyses of allelic series of *mHtt* KI mice revealed that such transcriptional changes strongly correlate with the length of CAG repeats and with age (Langfelder et al., 2016). It is not clear, however, which of the transcriptional alterations critically contribute to the physiopathology of HD and which ones are only epiphenomena of cell dysfunction or neurodegeneration. RARβ is one of the transcription factors, which expression gradually decreases with increasing CAG-length and age in *mHtt* KI mouse lines and is significantly downregulated in the striatum of HD patients (Hodges et al., 2006), raising the possibility that it may be responsible for a subset of transcriptional and functional changes in HD. Supporting such a hypothesis, we previously showed that RARβ is a direct or indirect regulator of genes controlling cell identity, calcium and cAMP signalling, cell morphology or mitochondrial functions (Niewiadomska-Cimicka et al., 2017) – all of them being deregulated in HD and animal models (Hodges et al., 2006; Langfelder et al., 2016; Luthi-Carter et al., 2000). In the present study, by using *in vitro* and *in vivo* approaches including different animal models, we identified a new, post-natal function of RARβ in neuroprotection of spMSNs, which may be correlated to the increased vulnerability of these cells in HD. Indeed, *Rarβ*^{-/-} mice display a post-natal loss of about 25% of Drd2 + spMSNs, with these cell numbers being reduced in the striatum of adult *Rarβ*^{-/-} mice, whereas they are unaffected in newborn *Rarβ*^{-/-} mice (see our previous study (Rataj-Baniowska et al., 2015)). Such postnatal, neuroprotective role of RARβ in spMSNs is further supported by: (i) increased apoptotic cell death in striatum of *Rarβ*^{-/-} mice, (ii) selective reduction of spMSNs in *Rarβ*[AAV9EGFPCre] mice with conditional ablation of RARβ in the adult striatum, (iii) selective reduction of spMSNs in *Rarβ*[Drd2Cre-/-] mice with spMSN-specific ablation of RARβ, (iv) a sensitizing effect in *Rarβ*^{-/-} mice to lose spMSNs in response to 3-NP, as well as (v) their neuroprotection by RARβ agonist in WT mice treated with 3-NP. Loss of Drd2 + spMSNs in *Rarβ*[AAV9EGFPCre] and in *Rarβ*[Drd2Cre-/-] mice also excludes the possibility that reduced number of spMSNs in *Rarβ*^{-/-} mice results solely from neurodevelopmental abnormalities leading in turn to enhanced sensitivity and degeneration of these cells in the adult. We cannot completely exclude that reduced counts of *Drd2* + cells may partially reflect lack of transcriptional activation of the *Drd2* gene by RARβ (Krezel et al., 1998; Niewiadomska-Cimicka et al., 2017; Samad et al., 1997), but this possibility appears less likely because of concomitant reduction of cells expressing pENK, a distinct marker of spMSNs as well as a 25% reduction of the total number of cells (DAPI+), 27% reduction of

Gad67 + MSNs and finally 23% reduction of cells expressing truncated *Rarβ* transcript in *Rarβ*^{-/-} mutants (these cells correspond to *Rarβ* expressing cells in WT conditions). In fact, deficits in global cell number and *Gad67* + MSNs would rather support a cumulative absence of both snMSN and spMSN populations. Indeed, we also observed a ~20% reduction of Drd1 + snMSNs in the striatum of adult *Rarβ*^{-/-} mice, though this deficit reflects a pre-natal function of RARβ in controlling development of Drd1 cells (Rataj-Baniowska et al., 2015). In agreement with this possibility, ~10% reduction of *Gad67* + cells was associated with loss of ~15% of *Drd2* + neurons following inactivation of *Rarβ* in post-natal striatum in *Rarβ*[AAV9EGFPCre] mice or in post-mitotic spMSNs in *Rarβ*[Drd2Cre-/-] mice. Reduced expression of Drd2 or cell loss could also contribute to the strong, 40% decrease of cells co-expressing Drd1 and Drd2 observed in mutant mice. Although this cell population represents only a small fraction of MSNs in dorsal and ventral striatum (5% and 15%, respectively), their reduction does not overtly affect global MSN counts, but it may have important consequence on functions controlled by Drd1 + ;Drd2 + double positive cells, which remain little understood to date.

Specificity of spMSN loss cannot be explained by selective expression of RARβ in this cell population, as our analyses show that RARβ is expressed in comparable numbers of snMSNs and spMSNs (which together encompass most of the MSN population, as revealed by co-localization of Drd1 + or Drd2 + transcripts with RARβ protein). In fact, our observations of a nearly ubiquitous expression of RARβ in MSNs contrasting with loss of only 15–19% of spMSNs (depending on animal model) suggest molecular diversity of striatal MSNs and existence of restricted subpopulation of spMSNs particularly susceptible to cell death in absence of RARβ. Alternatively, relatively low 15–19% reduction of MSNs restricted to spMSNs may correspond to a snap-shot of a dynamic neurodegenerative process which we analysed at about 12 weeks of age. Such process may evolve with age and we cannot exclude that at later phases also Drd1 + MSNs could be affected. Although this merits dedicated longitudinal study of aging, some insight can be already gained from progressive motor deficits associated with loss of 15% of spMSN at 20 weeks after RARβ inactivation in *Rarβ*[AAV9EGFPCre] mice. Such data support a long-term neuroprotective activity of RARβ, but also its selective effect limited to spMSNs. Further evidence comes also from exacerbated loss of *Drd2* + MSNs in *Rarβ*^{-/-} mice exposed to 3-NP death and neuroprotective activities of RARβ agonist and selective prevention of *Drd2* + cell loss in wild type mice treated with 3-NP, a pharmacological model of HD (see also below).

Molecular underpinnings of particular susceptibility of spMSNs to RARβ deletion remain unclear, but may involve deregulation of mitochondrial genes (as suggested by mitochondrial dysfunction in cultured *Rarβ*^{-/-} MSNs) together with downregulation of genes related to cAMP signaling like Pgc1α or Pde10a reported previously (Niewiadomska-Cimicka et al., 2017). For example, pharmacological studies reported that reduced Pde10a activity leads to selective increase in excitability of spMSN (Threlfell et al., 2009). Thus, reduction of Pde10a expression in *Rarβ*^{-/-} striatum could potentially lead to hyperactivity and associated high energy demand selectively in spMSN increasing their lethality due to mitochondrial insufficiency. Also, an increased susceptibility to stress could be conferred selectively to spMSNs by reduced expression of adenosine A2 receptor, a direct target of RARβ (Niewiadomska-Cimicka et al., 2017), known for its neuroprotective activities in spMSNs (Blum et al., 2003). These and other mechanisms remain to be investigated.

Collectively, our data demonstrate that loss of RARβ signalling is sufficient to cause Drd2 + MSN cell loss. This finding is particularly relevant for HD in the light of a recent single cell RNAseq study reporting that RARβ and its target genes are the most downregulated in both MSN types in 6-month old *mHtt* Q175KI and 9-week old R6/2 striatum (Lee et al., 2020). Thus, we speculate that compromised neuroprotective activity of RARβ in spMSNs could contribute to their loss observed in these mice at 16 months and 12 weeks, respectively (Slow et al., 2003; Smith et al., 2014). However, such cell loss is not frequently observed in

other animal models of HD, possibly because the threshold level of reduced RARβ expression and/or activity is not attained during the life span of those animals. In line with this possibility, motor deficits and a 15% reduction of spMSNs in conditional RARβ knockout mice were observed at 5 months after RARβ inactivation.

Despite similar deficits in numbers of spMSNs and snMSNs in adult *Rarβ*$^{-/-}$ striatum, our functional data support strong, selective dysfunction of the indirect (striatopallidal) pathway, as opposed to a relatively spared activity of the direct (striatonigral) pathway. Although such observations agree with classical models of basal ganglia function and pathology, more recent observations on spatial clustering of active striatal neurons raise further question about how such deficits may affect cluster-like patterns of spMSNs and snMSNs, which may be essential for movement control (Parker et al., 2018). Our data support compromised activity of spMSNs, but they lack network and temporal resolution necessary for such insight. Thus, haloperidol, a preferential antagonist of Drd2, induced strong catalepsy in WT mice, but such effect was dramatically decreased in *Rarβ*$^{-/-}$ mice. The blunted effect of haloperidol may reflect compromised activation of cAMP signalling, based on the evidence of a ~40% reduction in number of cFos-expressing cells in the striatum, which exceeds the 25% deficit in Drd2 + cell number. In support of a selective dysfunction of spMSNs is also the strongly blunted response to amphetamine, which is reminiscent of that observed in cocaine or methamphetamine-treated *Drd2*$^{-/-}$ mice (Baik et al., 1995; Kelly et al., 2008), whereas *Drd1*$^{-/-}$ mice display hyperactivity after amphetamine treatment (Karper et al., 2002; McDougall et al., 2005; Xu et al., 2000). In contrast to compromised spMSN pathway, a selective Drd1 agonist, SKF 81297, induced a similar level of motor activity and striatal cFos expression in WT and *Rarβ*$^{-/-}$ mice, suggesting that the striatonigral pathway is not overtly compromised in this challenge despite reduced number of snMSNs. This may possibly reflect some compensatory mechanisms resulting in the hyperactivity of snMSNs. Such hyperactivity could add to or synergise with reduced spMSN activity to increase snMSN/spMSN signaling disequilibrium. This could be determinant factor leading to spontaneous motor hyperactivity of *Rarβ*$^{-/-}$ and *Rarβ*^{AAV9EGFPCre} mice in actimetric cages as *Rarβ* was deleted in both spMSNs and snMSNs. Accordingly, spMSN-selective inactivation of *Rarβ* leading to reduced indirect pathway activity was not sufficient to induce this phenotype in *Rarβ*$^{Drd2-/-}$ mice. Interestingly, one of the earliest phenotypes observed in YAC128 mouse model of HD was hyperactivity of Drd1 + MSNs on evidence of enhanced sEPSCs, which was proposed to contribute to unbalanced signalling of striatonigral *vs* striatopallidal pathways (Andre et al., 2011). Such unbalanced signaling is also reflected by HD-like behavioral abnormalities in *Rarβ*$^{-/-}$ mice. Thus, locomotor coordination deficits in the rotarod and lower novelty-induced activity in the open field may correspond to reduced spMSN signalling since it has also been reported in HD mouse models (Bolivar et al., 2004; Luesse et al., 2001; Slow et al., 2003; Smith et al., 2014) and were present in *Rarβ*$^{Drd2Cre-/-}$ mice. Also, the spontaneous hyperactivity observed during the night phase of the light/dark cycle was similar to that observed in young R6/1, R6/2, Yac128 and 12-month old HttQ175 + /- HD mouse models (Bolivar et al., 2004; Luesse et al., 2001; Slow et al., 2003; Smith et al., 2014) and likely reflects remaining and enhanced snMSN activity as discussed. Importantly, graded transcriptional changes, including decreased expression *Rarβ* and its targets, that are associated with increasing sizes of CAG repeats and age of *mHtt* KI lines displayed strong spMSN bias (Langfelder et al., 2016; Lee et al., 2020). Such observations converge with our data supporting the idea that compromised RARβ signalling underlies selective dysfunction of spMSNs prior to their eventual cell death in HD.

Mitochondrial dysfunction compromising MSN activity and survival due to the high energetic demands of this cell type (Ferrante et al., 1991; Mitchell and Griffiths, 2003) and/or increased susceptibility to glutamatergic toxicity (Cepeda et al., 2001; Estrada Sanchez et al., 2008; Fernandes et al., 2007; Hodgson et al., 1999; Mattis et al., 2015; Zeron et al., 2002) may underlie the high vulnerability of striatal MSNs in HD.

Several potential mechanisms were suggested for this, including reduced SDH enzymatic activity, supported by data from HD patients (Browne et al., 1997; Gu et al., 1996; Tabrizi et al., 1999), and mHtt-expressing cultured neurons (Benchoua et al., 2006), or selective MSN cell death following inhibition of SDH by 3-NP in rodents and human (Ludolph et al., 1991; Page et al., 2000; Sun et al., 2002). MSN cell death in HD was also proposed to involve opening of mPTP, a calcium-dependent mitochondrial channel, leading to loss of mitochondrial potential and mitochondrial fragmentation followed by apoptotic cell death (Quintanilla et al., 2017). Our study provides evidence that RARβ is an important modulator of mitochondrial functions and its compromised signalling underlies mitochondrial dysfunction including reduced SDH enzymatic activity and dysregulated calcium homeostasis as causal factors of MSN vulnerability in HD. Accordingly, the size of mitochondria in *Rarβ*$^{-/-}$ MSNs was slightly, but consistently increased, possibly reflecting abnormal calcium homeostasis observed in different models of neurodegeneration including HD and associated with dysfunction of mPTP (Jin et al., 2013; Martinez-Vicente et al., 2010; Pastorino et al., 1999; Quintanilla et al., 2017). Increased number of defective mitochondria with disorganized or missing cristae, which we observed in *Rarβ*$^{-/-}$ striatum, were also reported in HD patients and animal models (Jin et al., 2013; Squitieri et al., 2010). Our respirometry analyses in Oxygraph together with reduced enzymatic SDH activity were consistent with reduced mitochondrial respiration and activity of complex II in *Rarβ*$^{-/-}$ striatum, abnormalities also observed in HD (Benchoua et al., 2006; Tabrizi et al., 1999). Consequently, subthreshold levels of the SDH inhibitor 3-NP induced significant loss of spMSNs in *Rarβ*$^{-/-}$ but not in WT striatum, whereas higher concentrations of 3-NP were lethal predominantly in *Rarβ*$^{-/-}$ mice. Importantly, loss of spMSNs contrasted with preservation of *Drd1* + snMSNs in 3-NP treated *Rarβ*$^{-/-}$ mice supporting specificity of neuroprotective role of RARβ in spMSNs as well as developmental, but not neurodegenerative origin of reduced number of snMSNs cells in *Rarβ*$^{-/-}$ striatum. In fact, in contrast to some previous rodent studies we did not observe decrease of snMSNs also in 3-NP treated WT mice. This may result from our specific experimental conditions selected in order to reveal susceptibility of *Rarβ*$^{-/-}$ mice. Accordingly, previous studies used long-term (5–28 days) treatments in rats (Page et al., 2000; Sun et al., 2002) or mice (Blum et al., 2003) in contrast to short term 2-days treatment in present study. Also, our mixed genetic background was different from those used previously as well as doses of 3-NP (30 or 50 mg/kg/injection) were lower than most of the doses used in different mice strains (100 mg/kg/injection or more) (Gabrielson et al., 2001). Increased vulnerability of mitochondria in *Rarβ*$^{-/-}$ mice was also supported by rapid loss of mitochondrial membrane potential, mitochondrial fragmentation and cell death in response to glutamate or thapsigargin-induced calcium overload in primary cultures of *Rarβ*$^{-/-}$ MSNs. Although it is unclear whether mitochondrial fragmentation and cell death observed *in vitro* concerns selectively spMSNs, the changes in bimodal distributions of Mitotracker signal in thapsigargin-treated WT *vs Rarβ*$^{-/-}$ MSNs support existence two neuronal populations out of which one is particularly susceptible to lose mitochondrial potential in *Rarβ*$^{-/-}$ cultures and may potentially reflect spMSN neurons. In line with the detrimental effects of compromised RARβ signalling on mitochondrial functions and cell survival, treatment with the RARβ agonist AC261066 prevented loss of mitochondrial depolarization, and eventual mitochondrial fragmentation and cell death in primary cultures of WT MSNs when challenged with glutamate. Such neuroprotective effects were not observed in *Rarβ*$^{-/-}$ cells known to also express RARγ, demonstrating RARβ-specificity of the AC261066 treatment, and the selective involvement of RARβ in neuroprotective activities. Furthermore, AC261066 partially rescued reduction of SDH activity and prevented loss of spMSNs in WT mice treated with 3-NP, which was associated with improvement of behavioral outcome in locomotor coordination and motor activity as measured, respectively, in the rotarod and open field tests.

5. Conclusion

This study provides evidence for a neuroprotective role of RARβ in adult striatal spMSNs. We show that absence of RARβ is sufficient to cause selective dysfunction and cell loss of spMSNs in RARβ-null (*Rarβ*$^{-/-}$) mice, but also in mice with a selective, AAV-mediated inactivation of RARβ in the adult striatum (*Rarβ*^{AAV9EGFPCre} mice). We also provide evidence on cell-autonomous nature of such control as spMSN loss was also observed following Drd2-specific deletion of *Rarβ* in *Rarβ*$^{Drd2-/-}$ mice. Our data support the hypothesis that mitochondrial injury as documented in *Rarβ*$^{-/-}$ striatum by morphological (swelling, disorganized cristae), molecular (reduced SDH enzymatic activity) and functional (reduced respiration) alterations, is a direct causal factor of increased vulnerability of mitochondria, which in stress conditions of calcium overload or glutamate excitotoxicity will lead to mitochondria depolarization, fragmentation, ROS production and cell death, as observed here in primary *Rarβ*$^{-/-}$ MSN cultures. Furthermore, treatment with an RARβ agonist prevented the adverse effects of glutamate excitotoxicity on mitochondria and prevented cell death in primary cultures of WT MSNs. spMSN cell loss in *Rarβ*^{AAV9EGFPCre} and *Rarβ*$^{Drd2-/-}$ mice, increased susceptibility of spMSNs to cell death in *Rarβ*$^{-/-}$ mice treated with subthreshold doses of 3-NP, as well as prevention of spMSN cell death with the RARβ agonist AC261066, all provide evidence for a neuroprotective role of RARβ *in vivo* and its selectivity for spMSNs. Thus, mitochondrial dysfunction and selective vulnerability of spMSNs observed in HD could reflect compromised signalling by RARβ reported in spMSNs of HD patients and corresponding animal models. Relevance of our data for HD physiopathology is also supported by HD-like behavioral deficits observed in *Rarβ*$^{-/-}$ and *Rarβ*^{AAV9EGFPCre} mice, and AC261066-mediated partial prevention of motor deficits in the 3-NP mouse model. Our present data linking RARβ and mitochondrial functions are further supported by the recent demonstration of a role of RARβ in mitochondrial dynamics during neurite outgrowth (Trigo et al., 2019), and in a more general context may explain the protective effects of the AC261066 RARβ agonist in cardiac ischemia/reperfusion injury (Marino et al., 2018), non-alcoholic fatty liver disease (Trasino et al., 2016a) or liver, pancreas and kidney protection in obese diabetic mice (Trasino et al., 2016b). Further studies of RARβ expression and functions in material from HD patients may contribute to a better understanding of peripheral tissue failure in HD, which is a frequent cause of death in this disease (for review see (Carroll et al., 2015; Sassone et al., 2009)).

Author contributions

Designed the study: W.K. with contribution of A.N.C., V.A.B and B. G.; supervised the experiments: W.K. and A.N.C.; performed experiments: M.R.B., M.C., A.N.C., V.A.B., V.F., A.L.C., R.A. and W.K.; analyzed data and prepared figures: M.R.B., M.C., N.Z., A.N.C., V.A.B. and W.K.; Wrote the manuscript: W.K. with input from M.R.B., M.C., N. Z., V.A.B., A.L.C., S.M. and B.G. Resources and text editing: W.K., P.D., S. M. and A.R.L.

Conflict of interest

S.M. owns equity in a gene therapy company (Gene Therapy Research Institution, Co., Ltd.) that commercializes the use of AAV vectors for gene therapy applications. To the extent that the work in this manuscript increases the value of these commercial holdings, there is a conflict of interest.

Appendix A. Supporting information

Supplementary data associated with this article can be found in the online version at doi:10.1016/j.pneurobio.2022.102246.

References

Albin, R.L., Reiner, A., Anderson, K.D., Dure, L.St, Handelin, B., Balfour, R., Whetsell Jr., W.O., Penney, J.B., Young, A.B., 1992. Preferential loss of striato-external pallidal projection neurons in presymptomatic Huntington's disease. Ann. Neurol. 31, 425–430.

Andre, V.M., Cepeda, C., Fisher, Y.E., Huynh, M., Bardakjian, N., Singh, S., Yang, X.W., Levine, M.S., 2011. Differential electrophysiological changes in striatal output neurons in Huntington's disease. J. Neurosci. 31, 1170–1182.

Baik, J.H., Picetti, R., Saiardi, A., Thiriet, G., Dierich, A., Depaulis, A., Le Meur, M., Borrelli, E., 1995. Parkinsonian-like locomotor impairment in mice lacking dopamine D2 receptors. Nature 377, 424–428.

Benchoua, A., Trioulier, Y., Zala, D., Gaillard, M.C., Lefort, N., Dufour, N., Saudou, F., Elalouf, J.M., Hirsch, E., Hantraye, P., et al., 2006. Involvement of mitochondrial complex II defects in neuronal death produced by N-terminus fragment of mutated huntingtin. Mol. Biol. Cell 17, 1652–1663.

Blum, D., Galas, M.C., Pintor, A., Brouillet, E., Ledent, C., Muller, C.E., Bantubungi, K., Galluzzo, M., Gall, D., Cuvelier, L., et al., 2003. A dual role of adenosine A2A receptors in 3-nitropropionic acid-induced striatal lesions: implications for the neuroprotective potential of A2A antagonists. J. Neurosci. 23, 5361–5369.

Bolivar, V.J., Manley, K., Messer, A., 2004. Early exploratory behavior abnormalities in R6/1 Huntington's disease transgenic mice. Brain Res. 1005, 29–35.

Brouillet, E., Jacquard, C., Bizat, N., Blum, D., 2005. 3-Nitropropionic acid: a mitochondrial toxin to uncover physiopathological mechanisms underlying striatal degeneration in Huntington's disease. J. Neurochem 95, 1521–1540.

Browne, S.E., Bowling, A.C., MacGarvey, U., Baik, M.J., Berger, S.C., Muqit, M.M., Bird, E.D., Beal, M.F., 1997. Oxidative damage and metabolic dysfunction in Huntington's disease: selective vulnerability of the basal ganglia. Ann. Neurol. 41, 646–653.

Carroll, J.B., Bates, G.P., Steffan, J., Saft, C., Tabrizi, S.J., 2015. Treating the whole body in Huntington's disease. Lancet Neurol. 14, 1135–1142.

Cepeda, C., Ariano, M.A., Calvert, C.R., Flores-Hernandez, J., Chandler, S.H., Leavitt, B. R., Hayden, M.R., Levine, M.S., 2001. NMDA receptor function in mouse models of Huntington disease. J. Neurosci. Res. 66, 525–539.

Chapellier, B., Mark, M., Bastien, J., Dierich, A., LeMeur, M., Chambon, P., Ghyselinck, N.B., 2002. A conditional floxed (loxP-flanked) allele for the retinoic acid receptor beta (RARbeta) gene. Genesis 32, 91–94.

Crittenden, J.R., Graybiel, A.M., 2011. Basal Ganglia disorders associated with imbalances in the striatal striosome and matrix compartments. Front Neuroanat. 5, 59.

Deng, Y.P., Albin, R.L., Penney, J.B., Young, A.B., Anderson, K.D., Reiner, A., 2004. Differential loss of striatal projection systems in Huntington's disease: a quantitative immunohistochemical study. J. Chem. Neuroanat. 27, 143–164.

Dubinsky, J.M., 2017. Towards an understanding of energy impairment in Huntington's disease brain. J. Huntington's Dis. 6, 267–302.

Erlander, M.G., Tillakaratne, N.J., Feldblum, S., Patel, N., Tobin, A.J., 1991. Two genes encode distinct glutamate decarboxylases. Neuron 7, 91–100.

Estrada Sanchez, A.M., Mejia-Toiber, J., Massieu, L., 2008. Excitotoxic neuronal death and the pathogenesis of Huntington's disease. Arch. Med. Res. 39, 265–276.

Etter, G., Krezel, W., 2014. Dopamine D2 receptor controls hilar mossy cells excitability. Hippocampus 24, 725–732.

Fernandes, H.B., Baimbridge, K.G., Church, J., Hayden, M.R., Raymond, L.A., 2007. Mitochondrial sensitivity and altered calcium handling underlie enhanced NMDA-induced apoptosis in YAC128 model of Huntington's disease. J. Neurosci. 27, 13614–13623.

Ferrante, R.J., Kowall, N.W., Richardson Jr., E.P., 1991. Proliferative and degenerative changes in striatal spiny neurons in Huntington's disease: a combined study using the section-Golgi method and calbindin D28k immunocytochemistry. J. Neurosci. 11, 3877–3887.

Gabrielson, K.L., Hogue, B.A., Bohr, V.A., Cardounel, A.J., Nakajima, W., Kofler, J., Zweier, J.L., Rodriguez, E.R., Martin, L.J., de Souza-Pinto, N.C., et al., 2001. Mitochondrial toxin 3-nitropropionic acid induces cardiac and neurotoxicity differentially in mice. Am. J. Pathol. 159, 1507–1520.

Ghyselinck, N.B., Dupé, V., Dierich, A., Messaddeq, N., Garnier, J.M., Rochette-Egly, C., Chambon, P., Mark, M., 1997. Role of the retinoic acid receptor beta (RARbeta) during mouse development. Int J. Dev. Biol. 41, 425–447.

Gong, S., Doughty, M., Harbaugh, C.R., Cummins, A., Hatten, M.E., Heintz, N., Gerfen, C. R., 2007. Targeting Cre recombinase to specific neuron populations with bacterial artificial chromosome constructs. J. Neurosci. 27, 9817–9823.

Goodliffe, J.W., Song, H., Rubakovic, A., Chang, W., Medalla, M., Weaver, C.M., Luebke, J.I., 2018. Differential changes to D1 and D2 medium spiny neurons in the 12-month-old Q175+/- mouse model of Huntington's Disease. PLoS One 13, e0200626.

Gu, M., Gash, M.T., Mann, V.M., Javoy-Agid, F., Cooper, J.M., Schapira, A.H., 1996. Mitochondrial defect in Huntington's disease caudate nucleus. Ann. Neurol. 39, 385–389.

Hodges, A., Strand, A.D., Aragaki, A.K., Kuhn, A., Sengstag, T., Hughes, G., Elliston, L.A., Hartog, C., Goldstein, D.R., Thu, D., et al., 2006. Regional and cellular gene expression changes in human Huntington's disease brain. Hum. Mol. Genet 15, 965–977.

Hodgson, J.G., Agopyan, N., Gutekunst, C.A., Leavitt, B.R., LePiane, F., Singaraja, R., Smith, D.J., Bissada, N., McCutcheon, K., Nasir, J., et al., 1999. A YAC mouse model for Huntington's disease with full-length mutant huntingtin, cytoplasmic toxicity, and selective striatal neurodegeneration. Neuron 23, 181–192.

Jin, Y.N., Yu, Y.V., Gundemir, S., Jo, C., Cui, M., Tieu, K., Johnson, G.V., 2013. Impaired mitochondrial dynamics and Nrf2 signaling contribute to compromised responses to oxidative stress in striatal cells expressing full-length mutant huntingtin. PLoS One 8, e57932.

Karper, P.E., De la Rosa, H., Newman, E.R., Krall, C.M., Nazarian, A., McDougall, S.A., Crawford, C.A., 2002. Role of D1-like receptors in amphetamine-induced behavioral sensitization: a study using D1A receptor knockout mice. Psychopharmacology 159, 407–414.

Kelly, M.A., Low, M.J., Rubinstein, M., Phillips, T.J., 2008. Role of dopamine D1-like receptors in methamphetamine locomotor responses of D2 receptor knockout mice. Genes Brain Behav. 7, 568–577.

Kim, J., Moody, J.P., Edgerly, C.K., Bordiuk, O.L., Cormier, K., Smith, K., Beal, M.F., Ferrante, R.J., 2010. Mitochondrial loss, dysfunction and altered dynamics in Huntington's disease. Hum. Mol. Genet 19, 3919–3935.

Krezel, W., Ghyselinck, N., Samad, T.A., Dupé, V., Kastner, P., Borrelli, E., Chambon, P., 1998. Impaired locomotion and dopamine signaling in retinoid receptor mutant mice. Science 279, 863–867.

Krzyzosiak, A., Szyszka-Niagolov, M., Wietrzych, M., Gobaille, S., Muramatsu, S., Krezel, W., 2010. Retinoid x receptor gamma control of affective behaviors involves dopaminergic signaling in mice. Neuron 66, 908–920.

Langfelder, P., Cantle, J.P., Chatzopoulou, D., Wang, N., Gao, F., Al-Ramahi, I., Lu, X.H., Ramos, E.M., El-Zein, K., Zhao, Y., et al., 2016. Integrated genomics and proteomics define huntingtin CAG length-dependent networks in mice. Nat. Neurosci. 19, 623–633.

Lee, H., Fenster, R.J., Pineda, S.S., Gibbs, W.S., Mohammadi, S., Davila-Velderrain, J., Garcia, F.J., Therrien, M., Novis, H.S., Gao, F., et al., 2020. Cell type-specific transcriptomics reveals that mutant huntingtin leads to mitochondrial RNA release and neuronal innate immune activation. Neuron 107, 891–908 e898.

Li, X.G., Okada, T., Kodera, M., Nara, Y., Takino, N., Muramatsu, C., Ikeguchi, K., Urano, F., Ichinose, H., Metzger, D., et al., 2006. Viral-mediated temporally controlled dopamine production in a rat model of Parkinson disease. Mol. Ther. 13, 160–166.

Liao, W.L., Tsai, H.C., Wang, H.F., Chang, J., Lu, K.M., Wu, H.L., Lee, Y.C., Tsai, T.F., Takahashi, H., Wagner, M., et al., 2008. Modular patterning of structure and function of the striatum by retinoid receptor signaling. Proc. Natl. Acad. Sci. USA 105, 6765–6770.

Ludolph, A.C., He, F., Spencer, P.S., Hammerstad, J., Sabri, M., 1991. 3-Nitropropionic acid-exogenous animal neurotoxin and possible human striatal toxin. Can. J. Neurol. Sci. Le. J. Can. Des. Sci. Neurol. 18, 492–498.

Luesse, H.G., Schiefer, J., Spruenken, A., Puls, C., Block, F., Kosinski, C.M., 2001. Evaluation of R6/2 HD transgenic mice for therapeutic studies in Huntington's disease: behavioral testing and impact of diabetes mellitus. Behav. Brain Res 126, 185–195.

Lund, B.W., Knapp, A.E., Piu, F., Gauthier, N.K., Begtrup, M., Hacksell, U., Olsson, R., 2009. Design, synthesis, and structure-activity analysis of isoform-selective retinoic acid receptor beta ligands. J. Med. Chem. 52, 1540–1545.

Lund, B.W., Piu, F., Gauthier, N.K., Eeg, A., Currier, E., Sherbukhin, V., Brann, M.R., Hacksell, U., Olsson, R., 2005. Discovery of a potent, orally available, and isoform-selective retinoic acid beta2 receptor agonist. J. Med. Chem. 48, 7517–7519.

Luthi-Carter, R., Strand, A., Peters, N.L., Solano, S.M., Hollingsworth, Z.R., Menon, A.S., Frey, A.S., Spektor, B.S., Penney, E.B., Schilling, G., et al., 2000. Decreased expression of striatal signaling genes in a mouse model of Huntington's disease. Hum. Mol. Genet 9, 1259–1271.

Marino, A., Sakamoto, T., Tang, X.H., Gudas, L.J., Levi, R., 2018. A retinoic acid beta2-receptor agonist exerts cardioprotective effects. J. Pharm. Exp. Ther. 366, 314–321.

Martinez-Vicente, M., Talloczy, Z., Wong, E., Tang, G., Koga, H., Kaushik, S., de Vries, R., Arias, E., Harris, S., Sulzer, D., et al., 2010. Cargo recognition failure is responsible for inefficient autophagy in Huntington's disease. Nat. Neurosci. 13, 567–576.

Mattis, V.B., Tom, C., Akimov, S., Saeedian, J., Ostergaard, M.E., Southwell, A.L., Doty, C.N., Ornelas, L., Sahabian, A., Lenaeus, L., et al., 2015. HD iPSC-derived neural progenitors accumulate in culture and are susceptible to BDNF withdrawal due to glutamate toxicity. Hum. Mol. Genet 24, 3257–3271.

McDougall, S.A., Reichel, C.M., Cyr, M.C., Karper, P.E., Nazarian, A., Crawford, C.A., 2005. Importance of D(1) receptors for associative components of amphetamine-induced behavioral sensitization and conditioned activity: a study using D(1) receptor knockout mice. Psychopharmacology 183, 20–30.

Mitchell, I.J., Griffiths, M.R., 2003. The differential susceptibility of specific neuronal populations: insights from Huntington's disease. IUBMB Life 55, 293–298.

Mochel, F., Durant, B., Meng, X., O'Callaghan, J., Yu, H., Brouillet, E., Wheeler, V.C., Humbert, S., Schiffmann, R., Durr, A., 2012. Early alterations of brain cellular energy homeostasis in Huntington disease models. J. Biol. Chem. 287, 1361–1370.

Mochel, F., Haller, R.G., 2011. Energy deficit in Huntington disease: why it matters. J. Clin. Invest 121, 493–499.

Niccolini, F., Pagano, G., Fusar-Poli, P., Wood, A., Mrzljak, L., Sampaio, C., Politis, M., 2018. Striatal molecular alterations in HD gene carriers: a systematic review and meta-analysis of PET studies. J. Neurol. Neurosurg. Psychiatry 89, 185–196.

Niewiadomska-Cimicka, A., Krzyzosiak, A., Ye, T., Podlesny-Drabiniok, A., Dembele, D., Dolle, P., Krezel, W., 2017. Genome-wide Analysis of RARbeta transcriptional targets in mouse striatum links retinoic acid signaling with huntington's disease and other neurodegenerative disorders. Mol. Neurobiol. 54, 3859–3878.

Niewiadomska-Cimicka, A., Schmidt, M., Ozyhar, A., Jones, D., Jones, G., Kochman, M., 2011. Juvenile hormone binding protein core promoter is TATA-driven with a suppressory element. Biochim Biophys. Acta 1809, 226–235.

Oliveira, J.M., 2010. Nature and cause of mitochondrial dysfunction in Huntington's disease: focusing on huntingtin and the striatum. J. Neurochem 114, 1–12.

Page, K.J., Besret, L., Jain, M., Monaghan, E.M., Dunnett, S.B., Everitt, B.J., 2000. Effects of systemic 3-nitropropionic acid-induced lesions of the dorsal striatum on cannabinoid and mu-opioid receptor binding in the basal ganglia. Exp. Brain Res. 130, 142–150.

Panov, A.V., Gutekunst, C.A., Leavitt, B.R., Hayden, M.R., Burke, J.R., Strittmatter, W.J., Greenamyre, J.T., 2002. Early mitochondrial calcium defects in Huntington's disease are a direct effect of polyglutamines. Nat. Neurosci. 5, 731–736.

Parker, J.G., Marshall, J.D., Ahanonu, B., Wu, Y.W., Kim, T.H., Grewe, B.F., Zhang, Y., Li, J.Z., Ding, J.B., Ehlers, M.D., et al., 2018. Diametric neural ensemble dynamics in parkinsonian and dyskinetic states. Nature 557, 177–182.

Pastorino, J.G., Marcineviciute, A., Cahill, A., Hoek, J.B., 1999. Potentiation by chronic ethanol treatment of the mitochondrial permeability transition. Biochem Biophys. Res Commun. 265, 405–409.

Paxinos, G., Franklin, K.B.J., 2001, The mouse brain in stereotaxic coordinates (Academic Press).

Quintanilla, R.A., Jin, Y.N., von Bernhardi, R., Johnson, G.V., 2013. Mitochondrial permeability transition pore induces mitochondria injury in Huntington disease. Mol. Neurodegener. 8, 45.

Quintanilla, R.A., Tapia, C., Perez, M.J., 2017. Possible role of mitochondrial permeability transition pore in the pathogenesis of Huntington disease. Biochem Biophys. Res Commun. 483, 1078–1083.

Rataj-Baniowska, M., Niewiadomska-Cimicka, A., Paschaki, M., Szyszka-Niagolov, M., Carramolino, L., Torres, M., Dollé, P., Krężel, W., 2015. Retinoic acid receptor β controls development of striatonigral projection neurons through FGF-dependent and meis1-dependent mechanisms. J. Neurosci. 35, 14467–14475.

Reiner, A., Albin, R.L., Anderson, K.D., D'Amato, C.J., Penney, J.B., Young, A.B., 1988. Differential loss of striatal projection neurons in Huntington disease. Proc. Natl. Acad. Sci. USA 85, 5733–5737.

Richfield, E.K., Maguire-Zeiss, K.A., Vonkeman, H.E., Voorn, P., 1995. Preferential loss of preproenkephalin versus preprotachykinin neurons from the striatum of Huntington's disease patients. Ann. Neurol. 38, 852–861.

Rochette-Egly, C., Gaub, M.P., Lutz, Y., Ali, S., Scheuer, I., Chambon, P., 1992. Retinoic acid receptor-beta: immunodetection and phosphorylation on tyrosine residues. Mol. Endocrinol. 6, 2197–2209.

Samad, T.A., Krezel, W., Chambon, P., Borrelli, E., 1997. Regulation of dopaminergic pathways by retinoids: activation of the D2 receptor promoter by members of the retinoic acid receptor-retinoid X receptor family. Proc. Natl. Acad. Sci. USA 94, 14349–14354.

Sassone, J., Colciago, C., Cislaghi, G., Silani, V., Ciammola, A., 2009. Huntington's disease: the current state of research with peripheral tissues. Exp. Neurol. 219, 385–397.

Slow, E.J., van Raamsdonk, J., Rogers, D., Coleman, S.H., Graham, R.K., Deng, Y., Oh, R., Bissada, N., Hossain, S.M., Yang, Y.Z., et al., 2003. Selective striatal neuronal loss in a YAC128 mouse model of Huntington disease. Hum. Mol. Genet 12, 1555–1567.

Smith, G.A., Rocha, E.M., McLean, J.R., Hayes, M.A., Izen, S.C., Isacson, O., Hallett, P.J., 2014. Progressive axonal transport and synaptic protein changes correlate with behavioral and neuropathological abnormalities in the heterozygous Q175 KI mouse model of Huntington's disease. Hum. Mol. Genet 23, 4510–4527.

Spektor, B.S., Miller, D.W., Hollingsworth, Z.R., Kaneko, Y.A., Solano, S.M., Johnson, J. M., Penney Jr., J.B., Young, A.B., Luthi-Carter, R., 2002. Differential D1 and D2 receptor-mediated effects on immediate early gene induction in a transgenic mouse model of Huntington's disease. Brain Res. Mol. Brain Res. 102, 118–128.

Squitieri, F., Falleni, A., Cannella, M., Orobello, S., Fulceri, F., Lenzi, P., Fornai, F., 2010. Abnormal Morphology of Peripheral Cell Tissues From Patients with Huntington disease. J. Neural Trans. 77–83.

Sun, Z., Xie, J., Reiner, A., 2002. The differential vulnerability of striatal projection neurons in 3-nitropropionic acid-treated rats does not match that typical of adult-onset Huntington's disease. Exp. Neurol. 176, 55–65.

Tabrizi, S.J., Cleeter, M.W., Xuereb, J., Taanman, J.W., Cooper, J.M., Schapira, A.H., 1999. Biochemical abnormalities and excitotoxicity in Huntington's disease brain. Ann. Neurol. 45, 25–32.

Threlfell, S., Sammut, S., Menniti, F.S., Schmidt, C.J., West, A.R., 2009. Inhibition of phosphodiesterase 10A increases the responsiveness of striatal projection neurons to cortical stimulation. J. Pharm. Exp. Ther. 328, 785–795.

Trasino, S.E., Tang, X.H., Jessurun, J., Gudas, L.J., 2016a. A retinoic acid receptor beta2 agonist reduces hepatic stellate cell activation in nonalcoholic fatty liver disease. J. Mol. Med. 94, 1143–1151.

Trasino, S.E., Tang, X.H., Jessurun, J., Gudas, L.J., 2016b. Retinoic acid receptor beta2 agonists restore glycaemic control in diabetes and reduce steatosis. Diabetes, Obes. Metab. 18, 142–151.

Trigo, D., Goncalves, M.B., Corcoran, J.P.T., 2019. The regulation of mitochondrial dynamics in neurite outgrowth by retinoic acid receptor beta signaling. Faseb J. 33, 7225–7235.

Valjent, E., Bertran-Gonzalez, J., Hervé, D., Fisone, G., Girault, J.A., 2009. Looking BAC at striatal signaling: cell-specific analysis in new transgenic mice. Trends Neurosci. 32, 538–547.

Xu, M., Guo, Y., Vorhees, C.V., Zhang, J., 2000. Behavioral responses to cocaine and amphetamine administration in mice lacking the dopamine D1 receptor. Brain Res. 852, 198–207.

Zeron, M.M., Hansson, O., Chen, N., Wellington, C.L., Leavitt, B.R., Brundin, P., Hayden, M.R., Raymond, L.A., 2002. Increased sensitivity to N-methyl-D-aspartate receptor-mediated excitotoxicity in a mouse model of Huntington's disease. Neuron 33, 849–860.